Nano Energy 119 (2024) 109046

Contents lists available at ScienceDirect

Nano Energy

journal homepage: www.elsevier.com/locate/nanoen

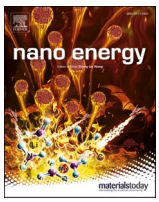

Review

Marine biomaterial-based triboelectric nanogenerators: Insights and applications

Yunmeng Li [a], Xin Liu [a], Zewei Ren [b], Jianjun Luo [c,d], Chi Zhang [c,d], Changyong (Chase) Cao [e], Hua Yuan [a,*], Yaokun Pang [a,*]

[a] State Key Laboratory of Bio-Fibers and Eco-Textiles, Collaborative Innovation Center of Marine Biobased Fiber and Ecological Textile Technology, Institute of Marine Biobased Materials, School of Materials Science and Engineering, Qingdao University, Qingdao 266071, PR China
[b] School of Advanced Materials and Nanotechnology, Academy of Advanced Interdisciplinary Research, Xidian University, Xi'an 710126, PR China
[c] Beijing Institute of Nanoenergy and Nanosystems, Chinese Academy of Sciences, Beijing 100083, PR China
[d] University of Chinese Academy of Sciences, Beijing 100049, PR China
[e] Laboratory for Soft Machines & Electronics, Department of Mechanical and Aerospace Engineering, Case Western Reserve University, Cleveland, OH 44106, USA

ARTICLE INFO

Keywords:
Marine biomaterials
Energy harvesting
Triboelectric nanogenerator
Renewable energy
Sustainability

ABSTRACT

The push for green and eco-friendly materials has intensified, driven by the mounting environmental concerns associated with traditional petroleum-based products. As land resources shrink and space for development narrows, marine biomaterials have emerged as a promising alternative over the past decades. Well-known for their vast availability, outstanding biocompatibility, impressive biodegradability, and minimal toxicity, marine biomaterials present an ideal foundation for developing eco-friendly triboelectric nanogenerators (TENGs). In this review, we present the evolution of TENGs based on marine biomaterials, from their core working principles to their multifaceted applications. We begin by elucidating the operational modes and foundational principles of TENGs. Next, we highlight the intrinsic qualities and advantages of marine biomaterials commonly utilized in TENG designs. Additionally, we discuss approaches adopted to amplify the efficacy of TENGs derived from marine biomaterials. A synthesis of documented applications of these TENGs from existing literature is then presented. We finally discuss the existing challenges and future directions in marine biomaterial-inspired TENGs.

1. Introduction

The ceaseless thirst for energy propels human civilization. Yet, our reliance on nonrenewable fossil fuels, which cater to nearly 80% of global energy needs, casts shadows of an impending energy crisis and environmental dilemmas [1–3]. The rise of emerging technologies like artificial intelligence, big data, and the Internet of Things (IoTs) has seen a surge in sensor deployments worldwide [4–6]. These sensors, albeit individually energy-efficient, cumulatively demand colossal power. Current battery technologies falter in sustainability, burdened by limited capacity, environmental concerns, and maintenance challenges. Hence, it's pivotal to innovate ways to transform ambient energy into electrical power, providing uninterrupted supply.

Numerous efforts have channeled into harvesting renewable energies, with mechanical energy, abundant in daily life and less weather-dependent, standing out [7–9]. Introduced by Wang's group in 2012, the triboelectric nanogenerator (TENG) capitalizes on the triboelectric effect and electrostatic induction [10–15]. TENGs offer cost-effectiveness, lightweight designs, user-centric operations, and eco-friendliness. They've been designed to harness energy from diverse sources, including wind, raindrops, and human motions, leading to TENG-based sensors serving varied purposes [16–22]. Furthermore, a large number of TENG-based self-powered sensors have been developed for various applications, such as health monitoring, environmental protection, medical care, security check, etc [23–28].

A TENG generally comprises three core components: a conductive electrode and both positive and negative tribo-materials. Currently, popular tribo-materials include synthetic polymers like polytetrafluoroethylene (PTFE), polyimide (PI), nylon, and polydimethylsiloxane (PDMS), known for their strong triboelectric charge. Yet, these non-renewable, non-biodegradable materials pose environmental and health threats, limiting their applicability in specific domains [29–33]. This necessitates the exploration of sustainable, renewable, and eco-friendly tribo-material alternatives.

* Corresponding authors.
E-mail addresses: yuanhua@qdu.edu.cn (H. Yuan), pangyaokun@qdu.edu.cn (Y. Pang).

https://doi.org/10.1016/j.nanoen.2023.109046
Received 6 October 2023; Received in revised form 24 October 2023; Accepted 27 October 2023
Available online 31 October 2023

Marine biomaterials, including chitosan, alginate, gelatin, and carrageenan, have gained prominence [34–36]. These biomaterials, derived from diverse marine sources like plants, animals, and microorganisms, offer broader accessibility and higher yield compared to terrestrial counterparts, without encroaching on freshwater or farmland. Their excellent biocompatibility, biodegradability, non-toxicity, and facile chemical modification have spurred scientific interest [37–40]. In 2014, Valentini et al. pioneered the use of marine biomaterials, specifically alginate, as tribo-materials in TENGs [41]. Subsequent research has proliferated marine biomaterial centric TENGs, marking it as a pivotal TENG research area (Fig. 1) [32,42]. Literature suggests that marine biomaterials aren't limited to the triboelectric layer; they're also fundamental in crafting transparent, stretchable TENGs using hydrogel electrodes. These TENGs are particularly promising in sectors like energy harvesting, environmental monitoring, and bio-medical implants.

In this review, we delve into recent advancements in the materials and applications of marine biomaterial-centric TENGs (Fig. 2). We commence by outlining the foundational principles and operational modes of TENGs. This is followed by highlighting the benefits and unique attributes of marine biomaterials frequently employed in TENGs, such as chitosan, alginate, gelatin, and carrageenan. We then explore the utilization of marine biomaterials in TENG electrodes. Our discussion extends to strategies enhancing the efficacy of these TENGs, encompassing techniques like physical doping, the design of surface morphology, ion incorporation, molecular surface refinement, and the layer-by-layer fabrication approach. Subsequently, we shed light on the prospective applications of marine biomaterial-driven TENGs in arenas like energy collection, innovative textiles, autonomous multifunctional sensors, interactive human-machine interfaces, and entirely biodegradable short-lived electronics. Finally, we address the prevailing challenges and anticipate the future trajectory of marine biomaterial-integrated TENG development.

2. Fundamentals of TENG

2.1. Working mechanism of TENG

The triboelectrification (CE) or contact electrification effect – a phenomenon prevalent in our daily lives and the natural world, has been known for 2600 years. This occurrence is omnipresent across various materials, ranging from polymers and metals to semiconductors, and interfaces, be it liquid-liquid, solid-solid, or solid-liquid [43,44]. Historically deemed a hazard due to its potential to cause discharges or explosions, CE has been meticulously avoided in many technological applications. Yet, in a game-changing discovery in 2012, Wang's team engineered the inaugural TENG, designed from Kapton film, polyester (PET) film, and thin strata of Au alloy films [10]. The underpinning mechanism of TENG is the coupling of CE and electrostatic induction, where is responsible for triboelectric charge generation on tribo-material surfaces, and electrostatic induction facilitates electrical output creation. Regular contact and separation of the paired tribo-materials yield an alternating current within TENG's external loop. Elaborating on this, Xu and colleagues postulated an electron-cloud-potential-well model, encompassing the entirety of CE phenomena across materials [45]. As shown in Fig. 3a<I>, prior to contact, the electron clouds of two materials remain distinct, with electrons firmly anchored to specific orbitals, courtesy of potential well-induced local trapping. On contact, a double-well potential, birthed from overlapping electron clouds, is observed under mechanical stress (Fig. 3a<II>). This leads to a decreased potential barrier, ushering electron transfers between atoms. Upon separation, due to energy barriers at ambient temperature, most transferred electrons linger as static charges on material surfaces (Fig. 3a<III>). Elevated temperatures cause heightened electron energy fluctuations, potentially prompting electrons to revert to their original atom or disperse into the atmosphere (Fig. 3a<IV>).

In a 2017 proposition, Wang emphasized the roots of TENG's fundamental principles in Maxwell's displacement currents, steered by

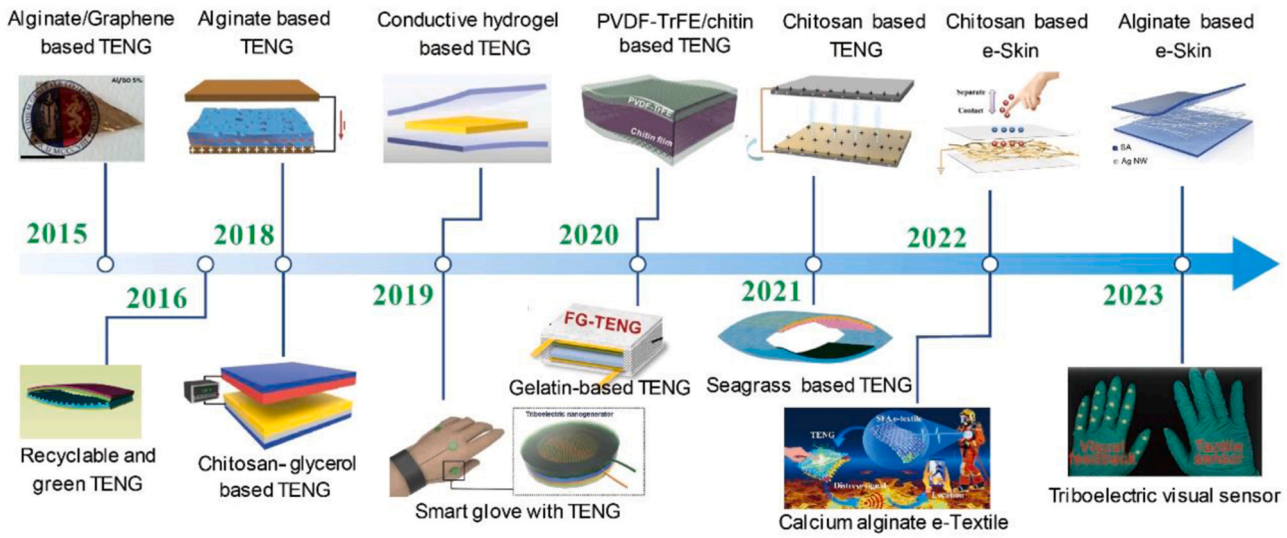

Fig. 1. The developments and examples of marine biomaterial-based TENGs. Alginate/GO based TENG. Reproduced with permission. [41] Copyright 2015, Wiley-VCH. Recyclable and green TENG. Reproduced with permission. [147] Copyright 2016, Wiley-VCH. Alginate film based TENG. Reproduced with permission. [129] Copyright 2018, Royal Society of Chemistry. Chitosan-glycerin based TENG. Reproduced with permission. [141] Copyright 2018, Elsevier. Hybrid ionic/electronic conductive hydrogel based TENG. Reproduced with permission. [92] Copyright 2019, Elsevier. Smart glove with TENG. Reproduced with permission. [156] Copyright 2019, National Institute for Materials Science in partnership with Taylor & Francis Group. PVDF-TrFE/chitin based TENG. Reproduced with permission. [157] Copyright 2020, American Chemical Society. Fish gelatin based TENG. Reproduced with permission. [124] Copyright 2020, American Chemical Society. Chitosan based TENG. Reproduced with permission. [158] Copyright 2021, Wiley-VCH. Seagrass based TENG. Reproduced with permission. [125] Copyright 2021, Elsevier. Transparent chitosan based TENG. Reproduced with permission. [149] Copyright 2022, Wiley-VCH. Calcium alginate based e-textile Reproduced with permission. [134] Copyright 2022, American Chemical Society. Alginate based e-Skin. Reproduced with permission. [143] Copyright 2023, Elsevier. Triboelectric visual tactile sensor. Reproduced with permission. [159] Copyright 2023, Wiley-VCH.

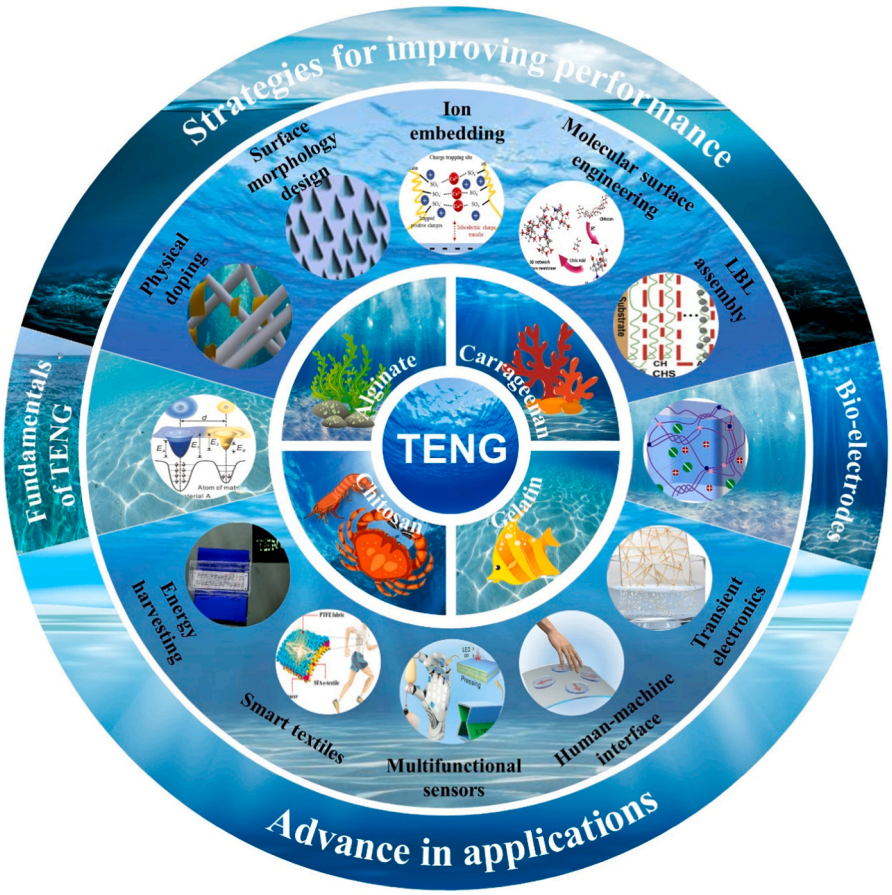

Fig. 2. Outline illustration of the review on marine biomaterial-based TENGs: fundamentals of TENG, strategies for improving performance, bio-electrodes, and applications. The major strategies for improving marine biomaterial-based TENG's performance include physical doping, surface morphology design, ion embedding, molecular surface engineering, and layer by layer (LBL) assembly. Applications include energy harvesting, smart textiles, self-powered multifunctional sensors, human-machine interface, and transient electronics.

the time-modulated polarization field and media polarization effects [46,47]. Essentially, the surface polarization in flux arises from the CE between two distinct dielectric substances. To succinctly represent its physical essence and calculate TENG's power output, a second term, P_S, was appended to the displacement vector D. Consequently, Maxwell's displacement current formula morphed into

$$J_D = \frac{\partial D}{\partial t} = \varepsilon \frac{\partial E}{\partial t} + \frac{\partial P_s}{\partial t}$$

where J_D is the displacement current, D represents the displacement field, and P indicates the polarization field. The first component ($\varepsilon \frac{\partial E}{\partial t}$) in this equation represents the displacement current from the time altered electric field and its induced medium polarization. Conversely, the second component ($\frac{\partial P_s}{\partial t}$), known as the Wang term, captures the displacement current resulting from the electrostatic charge-induced polarization field on surface. This term serves as the conceptual foundation and energy source of TENG. Advancing this, in 2021, Wang broadened and amplified Maxwell's electrodynamics equations, a move that might revolutionize wireless communication and precision signal processing (Fig. 3b) [48].

2.2. The operating modes of TENG

TENGs operate through four foundational modes, delineated by their electrode arrangement and the movement methods of the triboelectric layers to actualize the electrostatic induction process [49]. These four modes, as shown in Fig. 3c, are:

2.2.1. Contact-separation (CS) mode

As the quintessential configuration, this mode features two electrodes and two triboelectric layers (some models use the electrode substance for dual purposes: as an electrode and a triboelectric layer). The recurrent contact and separation of the two triboelectric layers foster a cyclical emergence and obliteration of potential difference between the two electrodes, subsequently driving an external current to equilibrate this potential difference.

2.2.2. Linear sliding (LS) mode

This mode engenders triboelectric charges due to the relative lateral movement at the contact interface, a departure from the CS mode. LS mode TENGs, especially those with a radial grating disk structure, are predominantly employed for the capture of rotational energy and flow energy from air or water, boasting a significant power output. However, their long-term stability remains a concern, as the continuous and high-frequency relative sliding of the two triboelectric surfaces can compromise the integrity of the TENG.

2.2.3. Single-electrode (SE) mode

This mode employs a solitary electrode. Its design is geared towards harnessing energy from objects in free motion, eliminating the requirement for electrode affixation. This makes it ideal for creating self-powered touch sensors or human-machine interfaces [50]. But a notable shortcoming of this mode is its comparatively subdued electrical output, owing to the inherent limitations stemming from the electrostatic shielding effect of the primary electrode.

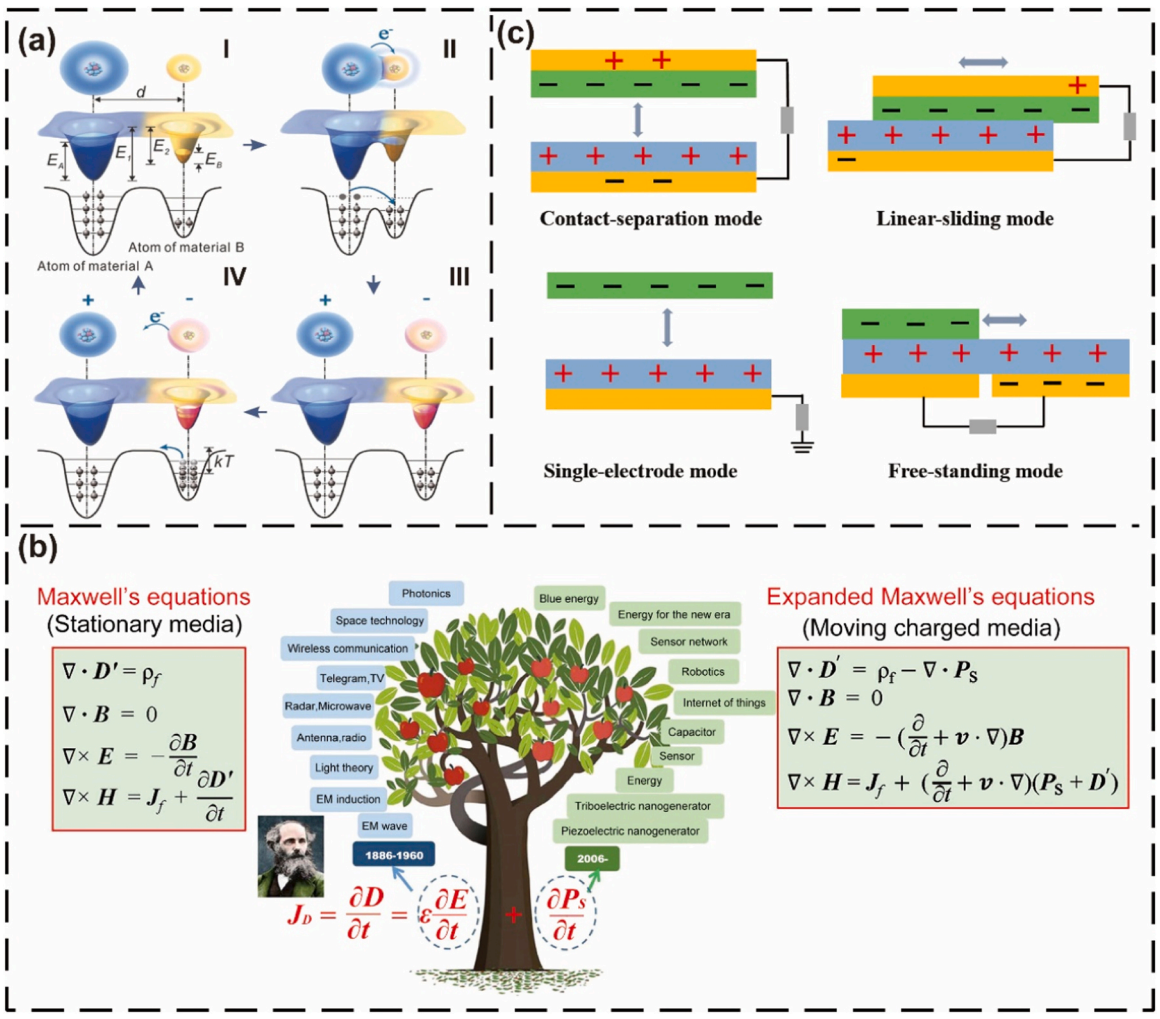

Fig. 3. Fundamental mechanism and theory of TENGs. (a) The electron cloud overlap model for contact-electrification. Reproduced with permission. [45] Copyright 2018, Wiley-VCH. (b) A comparison of the Maxwell's equations for stationary media and moving charged media. Reproduced with permission. [48] Copyright 2022, Elsevier. (c) The four fundamental working modes of TENGs.

2.2.4. *Freestanding triboelectric-layer (FT) mode*

This mode encompasses a mobile triboelectric layer and a symmetric pair of electrodes. The periodic movement of the triboelectric layer between these electrodes prompts electron movement, culminating in an alternating current (AC) output. Renowned for its superior energy conversion efficiency, the FT mode finds applications in diverse arenas like wave energy, vibrational energy, and rotational energy harvesting.

While each mode brings its unique strengths to the table, it's pivotal to acknowledge that TENGs aren't restricted to just one. In pragmatic scenarios, blending various modes offers an avenue to leverage their collective benefits, ensuring optimal functionality.

3. Marine biomaterials used for TENGs

3.1. *The advantages of marine biomaterials for TENGs*

Marine biomaterials, sourced from oceanic life forms like algae, seaweed, and shellfish, hold immense promise as eco-friendly alternatives for the upcoming generation of triboelectric devices. A quick overview of the recent advancements in marine biomaterial-based TENGs and their electrical efficacy can be found in Table 1. The significance of marine biomaterials in the realm of TENGs can be distilled into the subsequent core benefits:

3.1.1. *Abundant and renewable source*

Oceans, being vast reservoirs of biodiversity, furnish a plethora of biomass materials. These marine entities are not only plentiful but can also be harvested in an ecologically sustainable manner. Unlike terrestrial resources, which might entail considerable land utilization and pose ecological threats, marine biomass extraction preserves the ecological balance. Adding to their appeal, certain marine flora, like specific seaweeds, can grow prodigiously, with growth rates outstripping many terrestrial counterparts.

3.1.2. *Cost-effectiveness and scalability*

Marine biomaterials score high on economic viability due to their plenitude and easy accessibility, especially when juxtaposed with non-renewable resources. Their easy procurement, coupled with minimalistic processing requirements, ensures they are economically advantageous for TENG applications. Given their simplicity in production and processing, they also present a viable avenue for upscale TENG production.

3.1.3. *Prominent biodegradability*

With electronic waste burgeoning as a critical environmental challenge, marine biomaterials, inherently biodegradable, offer an eco-responsible solution. The current ecological zeitgeist underscores the urgency for sustainable electronics, and marine biomaterials, with their decomposition abilities, contribute towards an ecologically benign

Table 1
Research progresses of marine biomaterial-based TENGs.

Materials	TENG mode	Applications	Output voltage	Output current	Power density /loading resistance	Ref.
Alginate	CS mode	Self-powered sensors	21 V	0.48 μA	2.55 mW/m^2/ 700 kΩ	[162]
	SE mode	Infant care	5 V	/	/	[138]
	CS mode	Self-powered fire location system	3 V	/	/	[134]
	SE mode	Energy harvesting	145 V	8.7 μA	/	[163]
	SE mode	Energy harvesting and sensing	203.4 V	17.6 μA	0.98 W/m^2/ 4.7 MΩ	[87]
	CS mode	Energy harvesting	2.8 V	19 nA	/	[147]
	CS mode	Energy harvesting	100 V	0.35 nA	/	[160]
	CS mode	Wave energy harvesting	33 V	150 nA	/	[129]
	CS mode	Energy harvesting	288 V	40 nA	70.4 μW/cm^2/ 10 MΩ	[125]
	CS mode	Self-powered sensor	520 V	40 μA	/	[116]
Chitosan	CS mode	Energy harvesting	77 V	13 μA	22.4 μW/cm^2/ 5 MΩ	[164]
	CS mode	Energy harvesting	149 V	15 μA	/	[114]
	CS mode	Energy harvesting	9.7 V	393 nA	/	[165]
	CS mode	Self-powered gesture recognition	250 mV	/	/	[156]
	CS mode	Self-powered pressure sensor	/	500 nA	420 nW/cm^2/ 100 MΩ	[157]
	CS mode	Human motion detection	38 V	200 nA	3.3 mW/m^2/ 200 MΩ	[166]
	CS mode	Self-powered sensor	132 V	14 μA	/	[141]
	CS mode	Energy harvesting	55 V	0.6 μA	21.6 mW/m^2/ 67 MΩ	[167]
	CS mode	Human motion monitoring	145 V	1.03 μA	15.7 mW/m^2/ 100 MΩ	[95]
	CS mode	Self-powered tremor sensor	105 V	4 μA	/	[137]
	CS mode	Self-powered acetone sensor	0.7 V	/	/	[168]
	FT mode	Humidity detection	12 V	/	/	[169]
	CS mode	Self-powered tactile sensor	198.2 V	/	2.1 W/m^2/ 10 MΩ	[159]
	CS mode	Self-powered car speed sensor	16 V	30 nA	/	[121]
	SE mode	Self-powered sensor	50 V	0.3 μA	/	[149]
	CS mode	Energy harvesting	247.2 V	/	1.57 mW/cm^2/ 1 MΩ	[103]
	CS mode	Human machine interface	165 V	1.4 μA	160 mW/m^2/ 1 GΩ	[170]
	SE mode	Energy harvesting	107.7 V	10.6 μA	156 mW/m^2/ 9 MΩ	[171]
	CS mode	Energy harvesting	18 V	/	/	[158]
	SE mode	Self-powered sensor	31.3 V	1.8 μA	15.8 mW/m^2/ 100 MΩ	[135]
	SE mode	Energy harvesting	150 V	30 μA	2.0 W/m^2/ 10 MΩ	[92]
	CS mode	Energy harvesting	1.3 V	9 nA	/	[108]
	SE mode	Sitting posture monitoring	158 V	/	/	[172]
	CS mode	Human motion monitoring	168.2 V	7.6 μA	107.5 mW/m^2/ 10 MΩ	[173]
	CS mode	Smart fabric	1.24 V	110 nA	120 mW/m^2/ 2 kΩ	[174]
	SE mode	Self-powered written stroke recognition	182.4 V	4.8 μA	1.25 W/m^2/ 100 MΩ	[64]
	CS mode	Human motion and car movement monitoring	1080 V	27 μA	5.07 W/m^2/ 300 MΩ	[175]
Fish gelatin	SE mode	Energy harvesting and tactile sensing	22 V	400 nA	2.9 μW/cm^2/ 140 MΩ	[176]
	CS mode	Energy harvesting and human movement sensing	130 V	0.35 μA	45.8 μW/cm^2/ 10 MΩ	[124]
	SE mode	Human machine interface	105 V	7 μA	/	[177]
	CS mode	Human movement sensing	500 V	4 μA	100 μW/cm^2/ 100 MΩ	[113]
	CS mode	Self-powered ammonia gas sensor	400 V	50 μA	/	[140]
Carrageenan	CS mode	Self-powered breathing sensor	12.5 V	0.5 μA	/	[83]
	CS mode	Energy harvesting	17 V	/	0.15 mW/m^2/ 10 MΩ	[115]
	SE mode	Self-powered touch screen sensors	347.5 V	0.98 μA	/	[88]
	CS mode	Human machine interface	80 V	/	20 μW/cm^2/ 100 MΩ	[161]

electronic lifecycle.

3.1.4. *Amplified modifiability*

To enhance TENGs' power generation capabilities, chemical modification is pivotal. Marine biomaterials, replete with functional groups like carboxyl (-COOH), amino (-NH_2), and hydroxyl (-OH), are primed for facile modifications. Introducing electron-donating or withdrawing groups becomes simpler with these materials, furthering TENG

optimization.

3.1.5. Distinctive material properties

The intrinsic traits of marine biomaterials, such as alginate's solubility and filmogenic properties, make them impeccable for TENG applications. Marine biomaterials' innate attributes–lightweight nature, flexibility, transparency–dovetail perfectly with the prerequisites of wearable TENGs. Furthermore, their biocompatibility ensures they meld seamlessly with living systems, marking them as ideal for biocompatible TENGs employed in medical devices and wearables.

3.2. Properties of marine biomaterials as triboelectric layers

3.2.1. Alginate-based materials

Alginate is a widely used natural hydrophilic polysaccharide found within the cell wall matrix of diverse brown algae, serving a crucial function in enhancing the structural integrity of the cell wall. Alginate has gained extensive utilization in various industries [51,52], including the food and textile sectors, as well as the realm of medicine [53–55], owing to its exceptional attributes such as non-toxicity, biocompatibility, biodegradability, and affordability. Sodium alginate (SA) is one of the most widely used derivatives of alginate, and the molecular weights of commercially available SA range from 32, 000–400, 000 g/mol [56]. Chemically, the main structure of alginate is composed of two monomeric units: β-D-mannuronic acid (M unit) and α-L-glucuronic acid (G unit), which are homogeneously (MM or GG) or heterogeneously (MG or GM) linked through 1–4 glycosidic bonds (Fig. 4a). The content of the M unit and G unit, as well as their distribution in the polymer chain, are determined by the source of alginate, seasonal conditions, and extraction processes. These factors play a significant role in influencing the structures, molecular weights, and physicochemical properties of alginate. There are many free hydroxyl (-OH) and carboxyl (-COOH) groups distributed along the backbone of alginate, which renders it an optimal choice for chemical functionalization. So far, oxidation, sulfation,

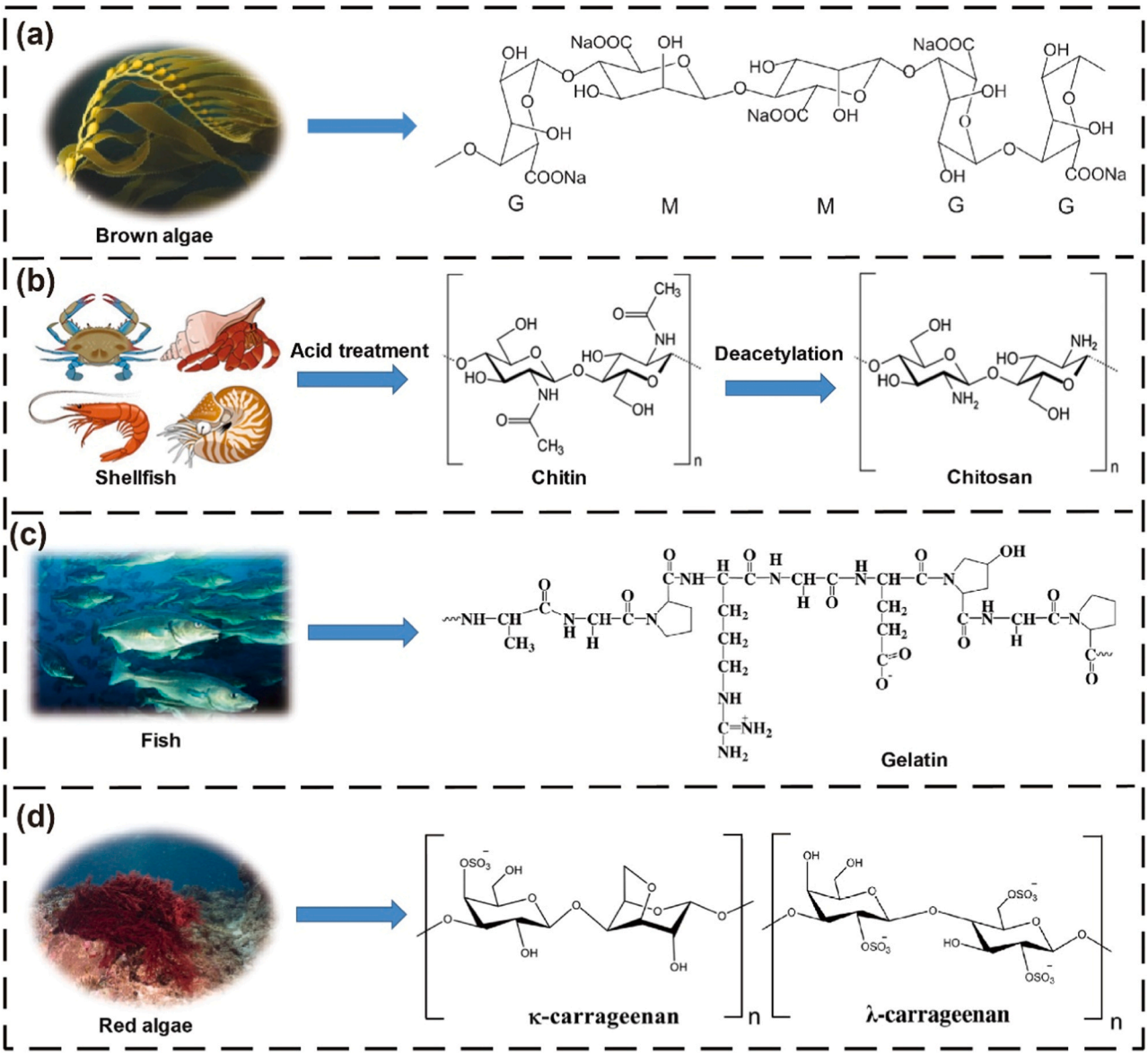

Fig. 4. Source and molecular formula of polysaccharides from marine organisms. (a) The source and molecular formula of sodium alginate. Reproduced with permission. [57] Copyright 2011, Elsevier. (b) The source and molecular formula of chitosan. Reproduced with permission. [59] Copyright 2017, Frontiers Media SA. (c) The source and molecular formula of gelatin. Reproduced with permission. [65] Copyright 2014, Elsevier. (d) The source and molecular formula of carrageenan. Reproduced with permission. [72–74] Copyright 2022, Wiley-VCH. Copyright 2014, Elsevier. (d) The source and molecular formula of carrageenan. Copyright 2009, Elsevier.

esterification, amidation, and grafting methods have been developed to modify the properties of alginate [57], such as solubility, hydrophobicity, and physicochemical characteristics. More importantly, alginate macromolecules can be easily used for the chelation of metal ions, such as Ca^{2+}, Fe^{3+}, Co^{2+}, and Ni^{2+}, forming a so-called "egg-box" structure, in which metal ion interacts with the G unit of two adjacent alginate macromolecules [58]. In 2014, Valentini et al. pioneered the application of alginate for TENGs [41]. They prepared Alginate/Graphene oxide hybrid films by solvent casting and served as the triboelectric layer in the TENG device. As an early-stage alginate-based triboelectric device, it showed a relatively low short-circuit current density of 1×10^{-4} mA·cm^{-2}, accompanied by an open-circuit voltage of 1.3 V.

3.2.2. Chitosan-based materials

Chitin stands as the world's second most abundant natural biopolymer after cellulose, which predominantly occurs in the outer skeleton of various shellfish, including crab, lobster, shrimp, and other crustacean shells. Chitosan is a linear polysaccharide compound consisting of β-(1−4) linked D-glucosamine and N-acetyl-D-glucosamine (Fig. 4b) [59]. The process of extracting chitosan involves two main stages: chitin extraction and chitin deacetylation [60]. Chemical hydrolysis and enzymatic treatment represent the primary techniques used to deacetylate, in which the hydrophobic acetyl groups are transformed into reactive and hydrophilic amino groups. Generally, the polymer with a degree of deacetylation (DD) beyond 50% is defined as chitosan, and less than 50% is considered chitin [61,62]. Most commercial chitosan has DD values in the range of 70%–90%. Among all the different parameters, DD and molecular weight exert the most significant influence on numerous physicochemical and biological properties of chitosan, such as solubility, flexibility, tensile strength, crystallinity, and so on [63]. Chitosan has made significant advances across various fields such as medicine, agriculture, and water engineering. More importantly, due to the existence of widely distributed amino groups with superior electron-donating ability, chitosan can be used as an excellent positive tribo-material for TENGs [31,32]. For instance, Zhang et al. reported a high-performance TENG based on a flexible and transparent chitin film, which tends to lose electrons and is positively charged easily [64]. The optimal chitin film based TENG exhibited great potential for energy harvesting and tactile sensing.

3.2.3. Fish gelatin-based materials

Gelatin is a water-soluble natural biopolymer obtained through heat denaturation and partial hydrolysis of collagen, which is abundantly contained in the bones, cartilage tissues, and skin of animals. Gelatin is basically composed of an abundant array of glycine, proline, and 4-hydroxy proline residues (Fig. 4c), with an elemental composition of 17% nitrogen, 25.2% oxygen, 6.8% hydrogen, and 50.5% carbon [65]. Gelatin is usually pale yellow or transparent, odorless, tasteless, and soluble in glycerin, hot water, and organic solvents such as citric acid [66]. It finds extensive applications in various fields, including biomedicine, food industry, packaging, pharmaceuticals, cosmetics, and photography. The global demand for gelatin is expected to reach 650 kilotons with a market of 4 billion US dollars by 2024 [67]. Generally, gelatin can be classified into two types depending on the pre-treatment of collagen: type A gelatin and type B gelatin [68–70]. The acid treatment gelatin known as Type A, derived from pig or fish skins, possesses an isoelectric point within the pH range of 6–9. Type B refers to alkaline treatment gelatin sourced from bovine hides, possessing an isoelectric point at pH 5. Approximately 71% of commercial gelatin is extracted from porcine skins and bovine hide due to their low-cost and substantial availability. However, the effects of bovine spongiform encephalopathy (BSE), foot-and-mouth disease (FMD), and swine influenzas have raised concerns about the utilization of gelatin extracted from these sources. Furthermore, pork-based gelatin has been restricted in Muslim and Jewish countries and communities, and bovine-derived gelatin is vulnerable to Hindu believers. Therefore, fish gelatin, derived from fish skins, scales, and bones, has received much attention as alternative source. As a bio-tribo-material, fish gelatin contains abundant amino acid residues with electron donor groups, endowing fish gelatin with a strong electron-losing ability during the friction process.

3.2.4. Carrageenan-based materials

Carrageenan is an anionic sulfated polysaccharide derived from the extracellular matrix of red algae seaweeds such as Chondrus, Eucheuma, Gigartina, and Hypnea. Structurally, it is formed by α-1,3 and β-1,4-glycosidic linkage of galactose residues i.e. D-galactose and 3,6-anhydro-D-galactose [71]. Carrageenan typically possesses ester sulfate content ranging from 15% to 40% and an average molecular weight exceeding 100 kDa. According to the number and position of the sulfate groups, carrageenan is divided into seven main types named after the Greek letters, among which κ-carrageenan, ι-carrageenan, and λ-carrageenan are the three major industrially important types (Fig. 4d) [72–74]. All types of carrageenan can dissolve in hot water to form a viscous transparent or slightly opalescent fluid solution, and their solubility is positively related to the content of sulfate units. It should be noted that λ-carrageenan can dissolve in cold water, but other types of carrageenan can only be dissolved in cold water by mixing certain metal ions. A unique physicochemical characteristic of carrageenan is its gel-forming ability. Below a critical temperature, the conformation of k-carrageenan and ι-carrageenan molecules in solution change from a random coil to helices, and eventually forms a 3-dimensional spanning network [75–77]. Unlike the k-carrageenan and ι-carrageenan, the λ-carrageenan is unable to form a gel and merely exhibits viscous behavior at all temperatures [78]. Due to the above-mentioned properties, carrageenan has aroused wide concern and has been widely used in various fields such as the food industry, pharmaceuticals, adsorption, biomedicine, printing, and electronics [78–82]. For example, Chen et al. reported a carrageenan-based double-network ionic hydrogel film with remarkable stretchability (>1100%) and commendable transparency (>80%) [83]. This film can be used as both the flexible electrode and a triboelectric layer and was combined with a fluorinated ethylene propylene film to form a self-powered tactile sensor. The main characteristics of marine biomaterials used in TENG are summarized in Table 2.

3.3. Marine biomaterials as triboelectric electrodes

Apart from the triboelectric layer, the electrode is also one of the most important components of TENG, which are usually conductive films (metal, graphene, conductive polymer, hydrogels, etc.). In general, electrodes in common TENGs haven't any special requirements apart from their conductivity. Nevertheless, for flexible and wearable applications, electrodes utilized in TENGs must fulfill several requirements: i) flexibility and stretchability to harvest human motion energy; ii) non-toxicity to guarantee the well-being and safety of users; iii) transparency for the visual transmission of information and esthetic purposes. Hydrogels, composed of highly deformable three-dimensionally cross-linked polymer networks and mobile ionic charge carriers, are the ideal choice for flexible TENGs with unique advantages such as high transparency, good conductivity, excellent stretchability, great biocompatibility, as well as easy integration with human skin [84–86].

Many marine biomass materials, such as alginate, carrageenan, and gelatin, have excellent gel-forming properties. These materials can absorb and retain large amounts of water, providing the hydrogel with its characteristic gel-like consistency. Jing and coworkers developed a self-healing dual-network hydrogel combined with dual-cross-linked poly(vinyl alcohol) (PVA) and SA (Fig. 5a) [87]. This innovative hydrogel was utilized as an ionic electrode in TENGs. Boronic ions play a crucial role in promoting the creation of a borax cross-linked PVA network, while Ca^{2+} ions induce the formation of a calcium cross/lined alginate structure. Attributed to the abundant reversible ionic bonds and hydrogen bonds, the hydrogel exhibits remarkable stretchability, capable of stretching up to 1000% strain, and it efficiently recovers from

Table 2
Characteristics of marine biomaterials used in TENGs.

Materials	Sources	Main moieties	Physicochemical properties	Extraction processes
Alginate	Brown algae	(1,4)-linked β-D-mannuronic acid and (1,4)-linked α-L-glucuronic acid	Alginates have good water solubility and are known to form viscous solutions or gels. Alginates can efficiently bind divalent cations.	(i) acidification of seaweeds; (ii) alkaline extraction using Na2CO3; (iii) solid/liquid separation; (iv) precipitation and (v) drying
Chitosan	Shrimp and crab	β-(1–4) linked D-glucosamine and N-acetyl-D-glucosamine	Chitosan is mainly characterized by the deacetylation degree and the molecular weight. Chitosan has poor solubility in water and most organic solvents, but it is soluble in most aqueous acid solutions. Chitosan films exhibit poor mechanical properties and low thermal stability.	(i) demineralization; (ii) deproteinization; (iii) deacetylation
Fish gelatin	Fish skins, scales, and bones	glycine, proline, and 4-hydroxy proline residues	Fish gelatin is usually pale yellow or transparent, odorless, tasteless, and soluble in glycerin, hot water, and organic solvents	(i) pretreatment of the raw material; (ii) extraction of the gelatin; (iii) purification and drying
Carrageenan	Red algae	(1,3) linked α-D-galactopyranose and (1,4) linked β-(3,6-anhydro)-D-galactopyranose	All types of carrageenan can dissolve in hot water to form a viscous transparent or slightly opalescent fluid solution. λ-carrageenan can dissolve in cold water, but other types of carrageenan can only be dissolved in cold water by mixing certain metal ions.	(i) hot alkaline treatment; (ii) ethanol precipitation

mechanical damage upon healing for 60 min. By optimizing the concentration of SA, the TENG exhibited a high output performance even though it was stretched to 200% of its original length, and it could easily power small electronics. In another similar work, Li et al. developed a self-healing polyacrylamide (PAM)/carrageenan double network (DN) hydrogel-based TENG [88]. As shown in Fig. 5b, the damaged DN hydrogel almost self-healed after 30 min with heating at 95 ℃ due to the unique thermally reversibility of k-carrageenan. Although the mechanical properties of the self-healed PAM/carrageenan DN hydrogel showed a significant decline compared with the original device, the output voltage of the fabricated TENG hardly deteriorates after self-healing.

For the majority of demonstrated flexible hydrogel-based TENGs, their output performance is limited by poor temperature tolerance [85,89,90]. In cold environments, large amounts of water inside hydrogels will be frozen, which will affect the electrical conductivity of the hydrogel, thus affecting the output performance of the TENG. To solve this problem, Wu et al. developed an anti-freezing gelatin/NaCl organohydrogel (GNOH) using a simple facile immersion technique in a glycerol/water binary solvent (Fig. 5c) [91]. The common gelatin hydrogel was completely frozen and transformed into a solid resembling ice with a white opaque appearance. In contrast, the GNOH was able to remain good mechanical strength and electrical conductivity even when exposed to extremely cold conditions (maintained at −20 ℃ for 24 h). Such a phenomenon can be attributed to the plentiful hydrogen bonds formed among water, glycerol, and gelatin. Thanks to the good anti-freezing ability of GNOH, the fabricated TENG demonstrates remarkable electrical output performance, enabling the efficient power supply to portable electronics, even under an extremely cold temperature (−20 ℃).

In comparison with metal electrodes, hydrogel exhibits a relatively lower level of conductivity. For the TENG application, the electrical conductivity significantly affects the charge induction and electrical transmission during the contact and separation cycles. Therefore, enhancing the conductivity of hydrogels becomes imperative. Nowadays, many approaches have been proposed to improve the conductivity of hydrogels, such as the addition of small salt molecules, conducting polymers, and metal materials. In Fig. 5d, Wang et al. combined an AgNW suspension with chitosan (CS) solutions, resulting in the formation of AgNW-embedded CS mixtures [92]. Subsequently, $AgNO_3$ or $CuSO_4$ solution was dropped on the mixture to produce interwoven structured CS hydrogels via complexation of functional groups of –OH and $–NH_2$ on chitosan chains with Ag^+ or Cu^{2+} cations. By optimizing the AgNWs concentration and precise selection of complexation metal ions, the fabricated hydrogel presented a high conductivity of 4.8 $mScm^{-1}$ (AgNWs-0.05%@CS/Ag). Furthermore, a sandwich-structured TENG was built with the hydrogel and PDMS to harvest motion energy.

In addition to hydrogel electrodes, the researchers have also developed marine biomass material-based laser-induced graphene (LIG) electrodes for TENG. Chitosan, with its hexagonal pyran ring serving as the fundamental structural unit, exhibits remarkable flame-retardant characteristics that form the foundation for the formation of LIG. As shown in Fig. 5e, three kinds of chitosan-based derivatives, including carboxymethyl chitosan (CMCS), chitosan oligosaccharide (COS), and chitosan hydrochloride (CSHC), were selected as carbon sources and converted into LIGs by a commercial infrared CO_2 laser [93]. The obtained LIGs exhibited good electrical properties with a low sheet resistance of 12.7 Ω sq^{-1}, thereby they were used as electrode materials for TENG. However, it should be noted that LIGs have a porous and interconnected structure that can be prone to mechanical degradation or disintegration under certain conditions, limiting their long-term stability and durability.

4. Strategies for improving marine biomaterial-based TENG performance

In recent years, due to the unique merits of marine biomaterials, they have attracted many researchers' attention in the field of TENGs. However, compared with the traditional tribo-materials, marine biomaterials usually have poor triboelectric performance which may limit the output performance of TENGs. It is critical to highlight that the output power of TENG is directly linked to the square of triboelectric charge density generated on contact surfaces. Thus, many studies have been conducted to augment the triboelectric charge density of marine biomaterials, thereby enhancing the output performance of TENG to make it a stable and sustainable power source for a wide range of applications. This section aims to make a detailed summary of reported methods for improving the output performance of marine biomaterial-based TENG.

4.1. Physical doping

One simple and effective strategy to enhance the output performance of TENGs is physical doping, in which nanomaterials are added to base materials to form composite materials. Some nanomaterials have strong electron-donating or electron-withdrawing capabilities, which can directly affect the surface charge density of the composite during contact electrification. Liu et al. developed TENGs using a composite of natural vermiculite (VMT) nanosheets with alginate fibers (Fig. 6a) [94]. A simple crushing and stripping method was applied to fabricate VMT nanosheets. The obtained VMT nanosheets exhibited a negatively charged nature because some trivalent Al^{3+} partially replaces the central tetravalent Si^{4+} of the tetrahedral silicate in VMT. The output voltage

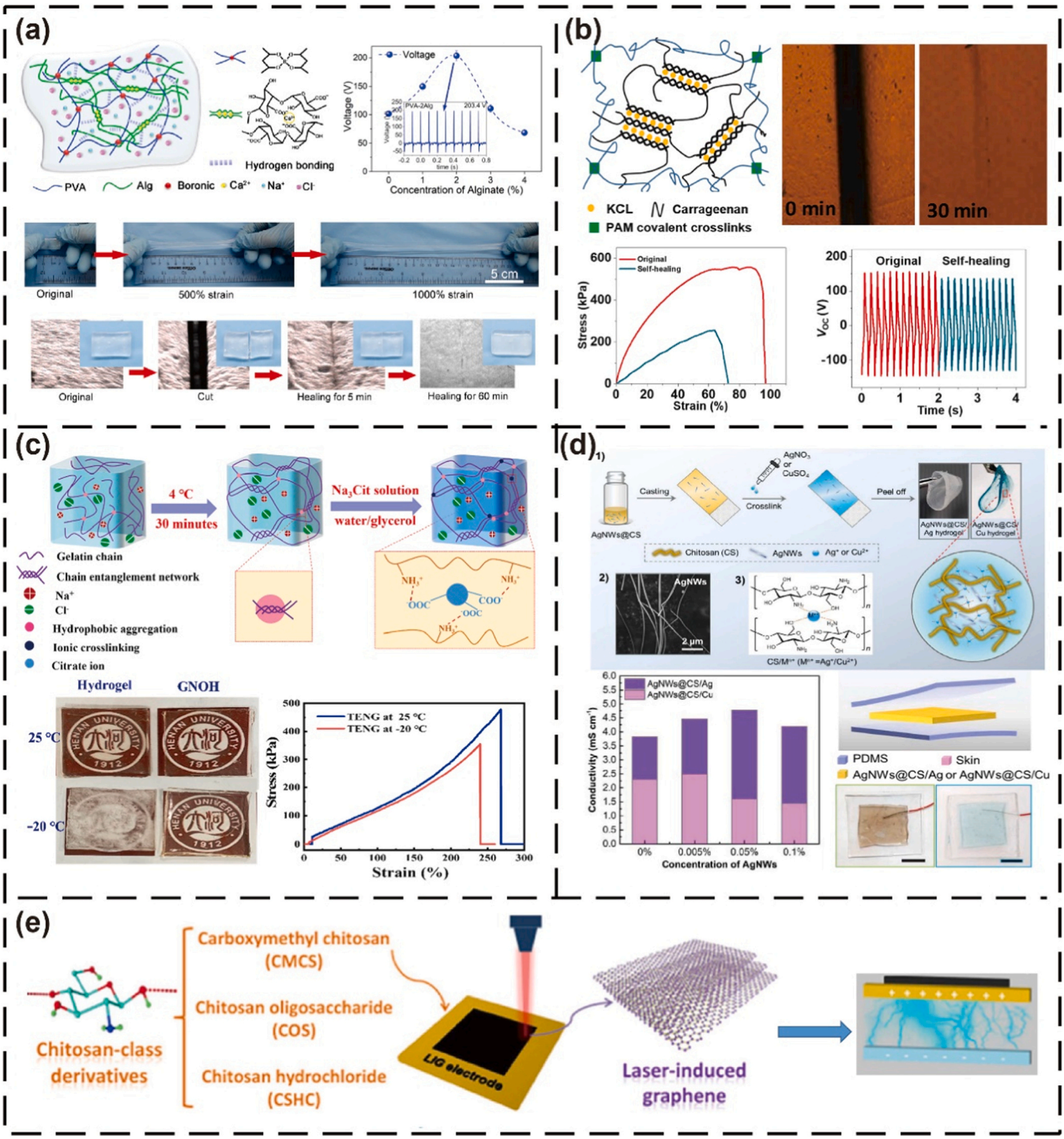

Fig. 5. Marine biomaterials as triboelectric electrodes. (a) A Self-healing dual-network hydrogel combined with dual-cross-linked PVA and SA with good tensile properties. Reproduced with permission. [87] Copyright 2020, American Chemical Society. (b) A self-healing PAM/carrageenan double DN hydrogel-based TENG. Reproduced with permission. [88] Copyright 2022, Elsevier. (c) An anti-freezing gelatin/NaCl organohydrogel (GNOH) using a simple facile immersion technique in a glycerol/water binary solvent. Reproduced with permission. [91] Copyright 2022, Elsevier. (d) By optimizing the concentration of AgNWs and precisely selecting the complex metal ions, the hydrogels with excellent properties were prepared, and a sandwich structure TENG was constructed with hydrogels and PDMS to collect movement energy. Reproduced with permission. [92] Copyright 2019, Elsevier. (e) Marine biomass material-based LIG electrodes for TENG. Reproduced with permission. [93] Copyright 2023, American Chemical Society.

and current of the TENG with a composite film filled with 5 g VMT nanosheets reached a peak value of 270 V/1 μA, while that of the pure alginate fiber film was only 120 V/0.4 μA. Kim et al. designed a remarkably enhanced biofriendly chitosan-based TENG using a highly porous diatom frustule as a biocompatible additive (Fig. 6b) [95]. Due to the high surface area, micro/nanoscale particle size, and high porosity, the diatom frustule can significantly enhance electro-positivity and surface properties of the composite film. The chitosan-diatom-based TENG demonstrated an impressive power density of 15.7 mW/m^2, surpassing the power density of pure chitosan by 3.7 times.

Another kind of commonly used filler is high dielectric nanomaterials, such as SiO_2, TiO_2, and $CaCu_3Ti_4O_{12}$ (CCTO), which can

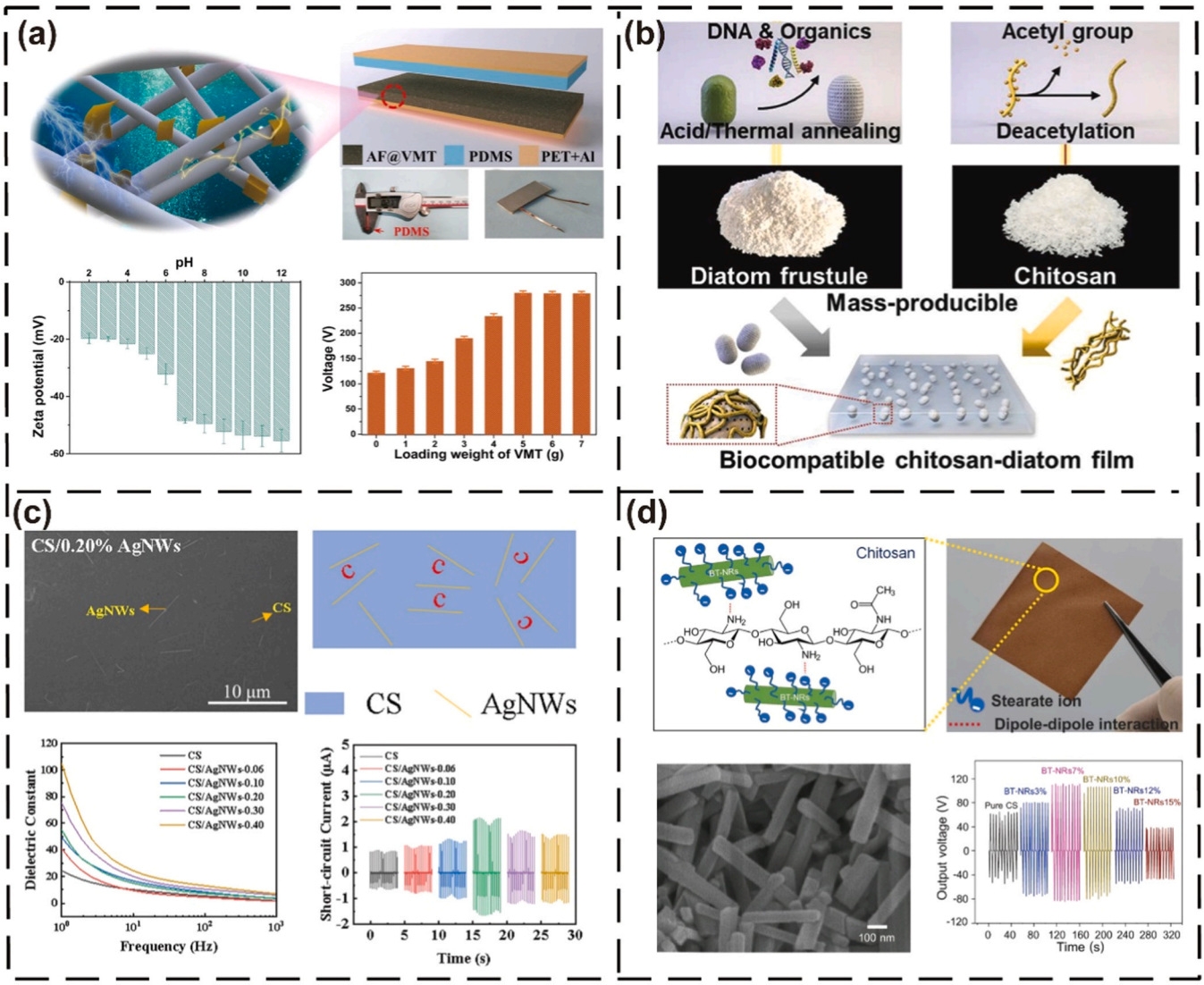

Fig. 6. Physical doping of marine biomaterials. (a) Developed TENGs using a composite of natural VMT nanosheets with alginate fibers. Reproduced with permission. [94] Copyright 2023, Springer nature. (b) A remarkably enhanced biofriendly chitosan-based TENG using a highly porous diatom frustule as a biocompatible additive. Reproduced with permission. [95] Copyright 2020, Elsevier. (c) Developed TENGs using a composite of AgNWs with chitosan. Reproduced with permission. [102] Copyright 2023, Royal Society Of Chemistry. (d) Piezoelectric $BaTiO_3$ nanorods (BT-NRs) via the salt flux-assisted method. Reproduced with permission. [103] Copyright 2021, Elsevier.

augment the relative permittivity of the base material [96–98]. This promising approach can be effectively applied to optimize marine biomaterial-based TENGs as well. For example, Yar et al. filled chitosan with various natural clays, including sepiolite, bentonite, and kaolin. The experimental results demonstrated that the clay particles have a substantial impact on the dielectric constant of the composite film. The output voltage of chitosan-based TENG with 3 wt% sepiolite, 1 wt% bentonite, and 1 wt% kaolin reached a peak value of 863, 996, and 963 V, while that of the pure chitosan film was only 400 V. Except for the high dielectric nanomaterials, conductive materials can also be used to enhance the relative permittivity of base materials [99–101]. A good example of this case was that Zhang et al. developed TENGs using a composite of AgNWs with chitosan [102]. As shown in Fig. 6c, single AgNWs were uniformly dispersed across the composite film, creating numerous parallel microcapacitors between adjacent AgNWs wrapped by the chitosan. With the increase of AgNWs content, the dielectric constant of composite films exhibited an increasing trend, and a maximum short-circuit current of 2.3 uA was achieved when the content of AgNWs is 0.20%.

Additionally, by filling piezoelectric materials into the base material, a hybrid piezo/triboelectric nanogenerator can be created, resulting in a significant enhancement of their output performance. Pongampai et al. synthesized piezoelectric $BaTiO_3$ nanorods (BT-NRs) via the salt flux-assisted method (Fig. 6d) [103]. The BT-NRs were treated with stearic acid to improve their dispersion in the chitosan matrix. When the weight of the BT-NRs is 7 wt%, the open-circuit voltage and short-circuit current reach the maximum values of 111.4 V and 21.6 μA/cm^2, respectively, which are 1.8 and 1.6 times greater than those of the TENG built with pure chitosan. The hybrid nanogenerator essentially generated its electrical output through the combination of two primary phenomena. One source of the electrical generation arose from the triboelectricity of the TENG in vertical contact-separation mode. Simultaneously, a second source emerged as piezoelectric charge induction within the chitosan/BT-NRs composite film during the compressing state. Therefore, the introduction of piezoelectric additives can improve the total electrical output performance of the TENG.

4.2. Surface morphology design

The surface morphology of the two frictional interfaces is a critical parameter in determining the surface charge density of triboelectric layers. Enhancing the output performance of TENG can be significantly achieved through surface morphological modifications. Researchers have used various manufacturing techniques to construct micro/nanostructures on the friction surface [104–107], which can effectively improve the surface roughness of the triboelectric layers, leading to a substantial increase in their effective contact area.

For optimized triboelectric power generation, Wang et al. introduced a laser treatment method to modify the surface properties of pure chitosan films [108]. As shown in Fig. 7a, the focused laser beam has the capability to induce nanoscale wrinkles on the chitosan film surface, and the surface morphology became coarser as the laser pulse count increased. After undergoing laser processing, the TENG experienced a notable enhancement in both output voltage and current, and the highest values were achieved when the chitosan film was treated by 4200 pulses. However, continuing to increase the number of pulses could cause the film to heat up excessively and promote surface charge diffusion in the chitosan film, resulting in less efficient TENG outputs. Furthermore, Zheng et al. utilized the freeze-drying technique to prepare chitosan aerogels with micro/nanostructures on friction surfaces to improve the triboelectric effect (Fig. 7b) [109]. The fabricated chitosan aerogel film displayed an interconnected 3D porous structure with a high surface area. In comparison with the TENG based on dense chitosan film, the TENG composed of spongy polymer films indicated an effective enhancement in output performance.

Some plant leaves exhibit superhydrophobic property with low adhesion, thanks to their distinct micro/nanostructure found on the surface. In comparison with sophisticated conventional micro/nanofabrication methods, directly replicating the micro/nanostructures of leave surfaces using soft lithography technology is a green and low-cost method [110,111]. Shi et al. fabricated a leaf microstructure-inspired

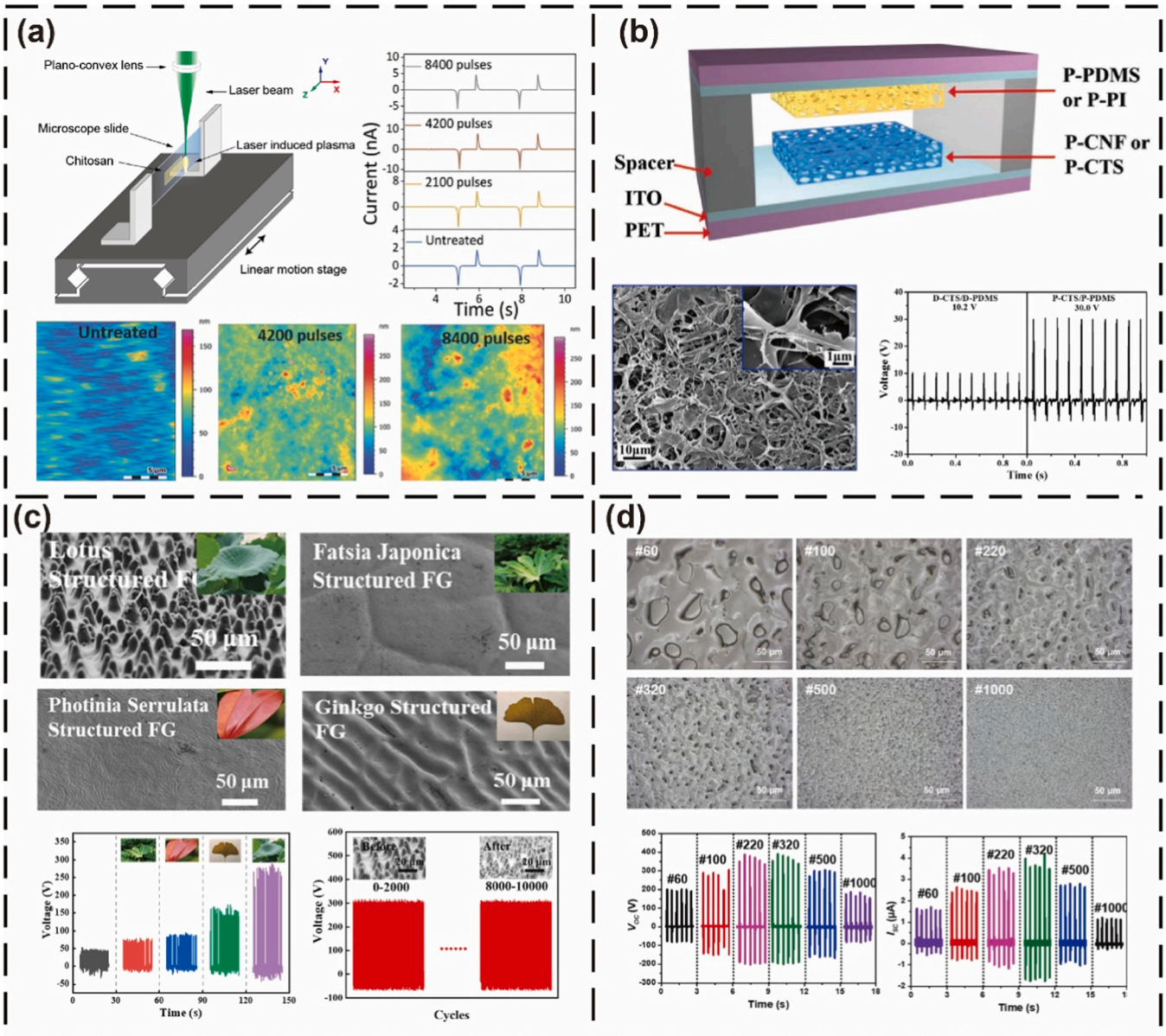

Fig. 7. Surface morphology design. (a) A laser treatment method to modify the surface properties of pure chitosan films. Reproduced with permission. [108] Copyright 2018, Wiley-VCH. (b) Utilized the freeze-drying technique to prepare chitosan aerogels with micro/nanostructures on friction surfaces. Reproduced with permission. [109] Copyright 2018, Wiley-VCH. (c) A leaf microstructure-inspired fish gelatin-based TENG. Reproduced with permission. [112] Copyright 2023, Elsevier. (d) Sandpapers as molds to fabricate microstructures on fish gelatin film's surface. Reproduced with permission. [113] Copyright 2021, Elsevier.

fish gelatin-based TENG through the facile replication of the microstructures of natural leaves (Fig. 7c) [112]. Four common plant leaves as effective microstructural molds were utilized to fabricate pyramid-like, square, groove, and grating microstructures, respectively. The TENG using lotus leaf as a mold with pyramidal microstructures showed the highest power generation performance, which was up to 6 times to the non-structured TENG. In addition, the fabricated TENG exhibited great electrical stability and there hasn't shown obvious damage of the film microstructure after ten thousand cyclic tests. In another example, Sun et al. used sandpapers as molds to fabricate microstructures on fish gelatin film's surface [113]. As shown in Fig. 7d, by utilizing sandpapers with various meshes, the roughness of the fish gelatin film can be easily adjusted, and it was found that the 320-mesh sandpaper yielded the most optimal output performance for the TENG.

4.3. Ion embedding

Although the physical doping method has been widely employed to improve the output performance of TENGs, it is difficult to achieve homogeneous dispersion of solid nanofillers in a polymer matrix, which may destroy the mechanical properties of the composite film. In this regard, embedding liquid ions is an excellent strategy to improve triboelectric properties for the tribo-material of TENGs.

Charoonsuk and co-workers employed a simple cationic salts embedding method to fabricate a chitosan/$CaCl_2$ film with good flexibility and transparency (Fig. 8a) [114]. In their work, the $CaCl_2$ solution was slowly added into the CS solution to ensure the homogeneous ionic distribution. A spring-assisted TENG was designed using the chitosan/$CaCl_2$ film and Teflon film as tribo-materials. The maximum voltage of

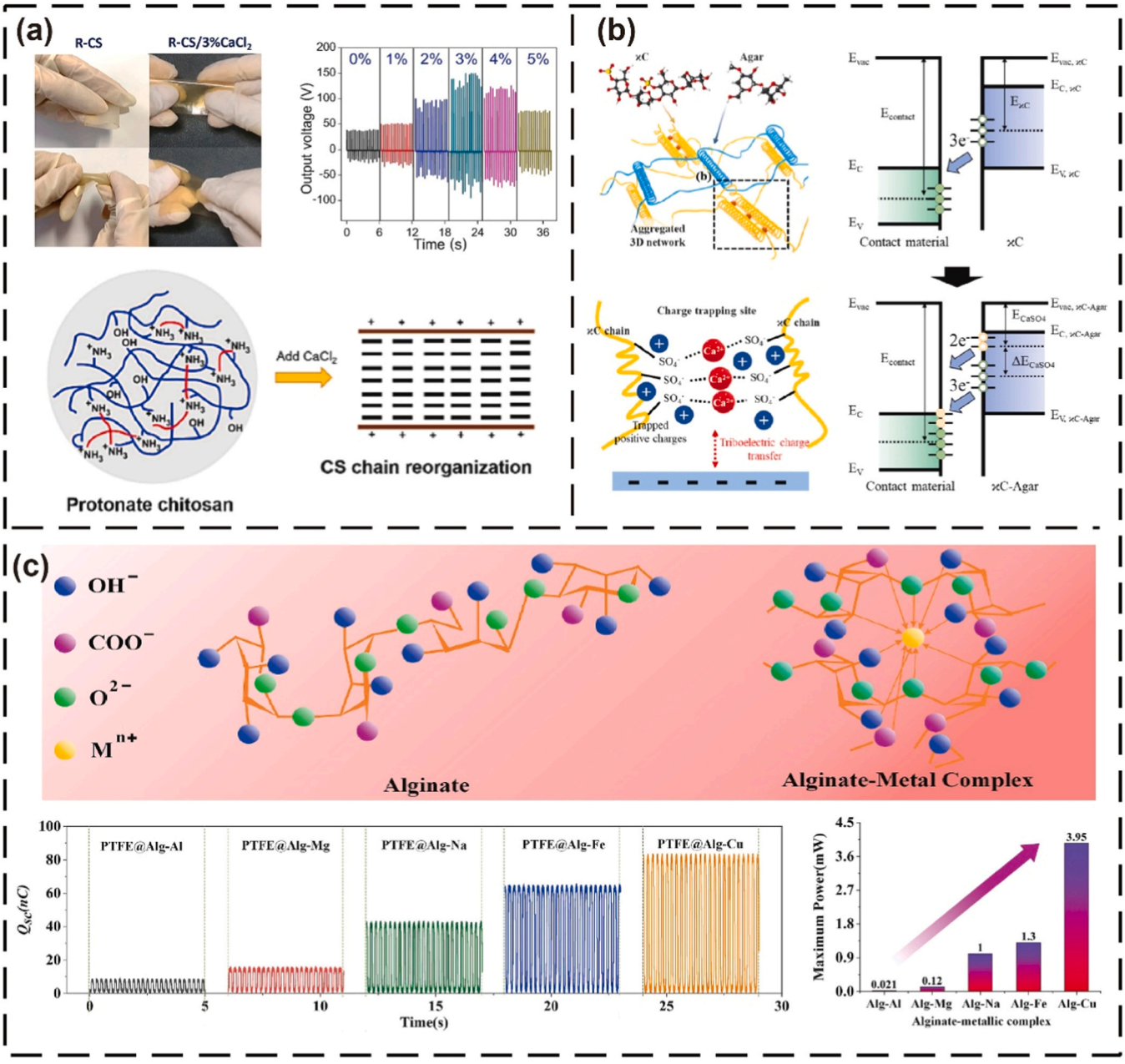

Fig. 8. Ion embedding. (a) A simple cationic salts embedding method to fabricate a chitosan/$CaCl_2$ film with good flexibility and transparency. Reproduced with permission. [114] Copyright 2022, Elsevier. (b) $CaSO_4$ salts into ϰ-carrageenan-agar (ϰC-Agar) to form a three-dimensional (3D) aggregated network composite. Reproduced with permission. [115] Copyright 2022, Elsevier. (c) A series of alginate-metallic complexes as tribo-materials. Reproduced with permission. [116] Copyright 2020, Elsevier.

150 V was obtained when the w/v percentage of $CaCl_2$ was 3%, which is 4 times that of pristine chitosan TENG. By adding $CaCl_2$, the chitosan polymer chains are reorganized, and NH_3^+ functional groups are rearranged on the chitosan surface. In another work, Kang et al. introduced $CaSO_4$ salts into ϰ-carrageenan-agar (ϰC-Agar) to form a three-dimensional (3D) aggregated network composite as a high-performing tribo-material (Fig. 8b) [115]. As shown in the energy band diagrams, high concentration Ca^{2+} cations and sulfate ester group in the composite dominantly increase charge trapping sites, providing additional electron-unoccupied states and leading to the high electron-donating property of the composite.

As mentioned in Section 3.2.1, alginate has the ability to bind with diverse cations to form an alginate metal complex. Based on this characteristic, Xia et al. prepared a series of alginate-metallic complexes as tribo-materials (Fig. 8c) [116]. The experiment results revealed that the alginate-metallic complex is a good positive tribo-material with a strong ability to lose electrons. The electrical output amplitude increases following the series of aluminum alginate (Alg-Al), magnesium alginate (Alg-Mg), sodium alginate (Alg-Na), ferric alginate (Alg-Fe), and copper alginate (Alg-Cu). The variation in the triboelectric characteristics of

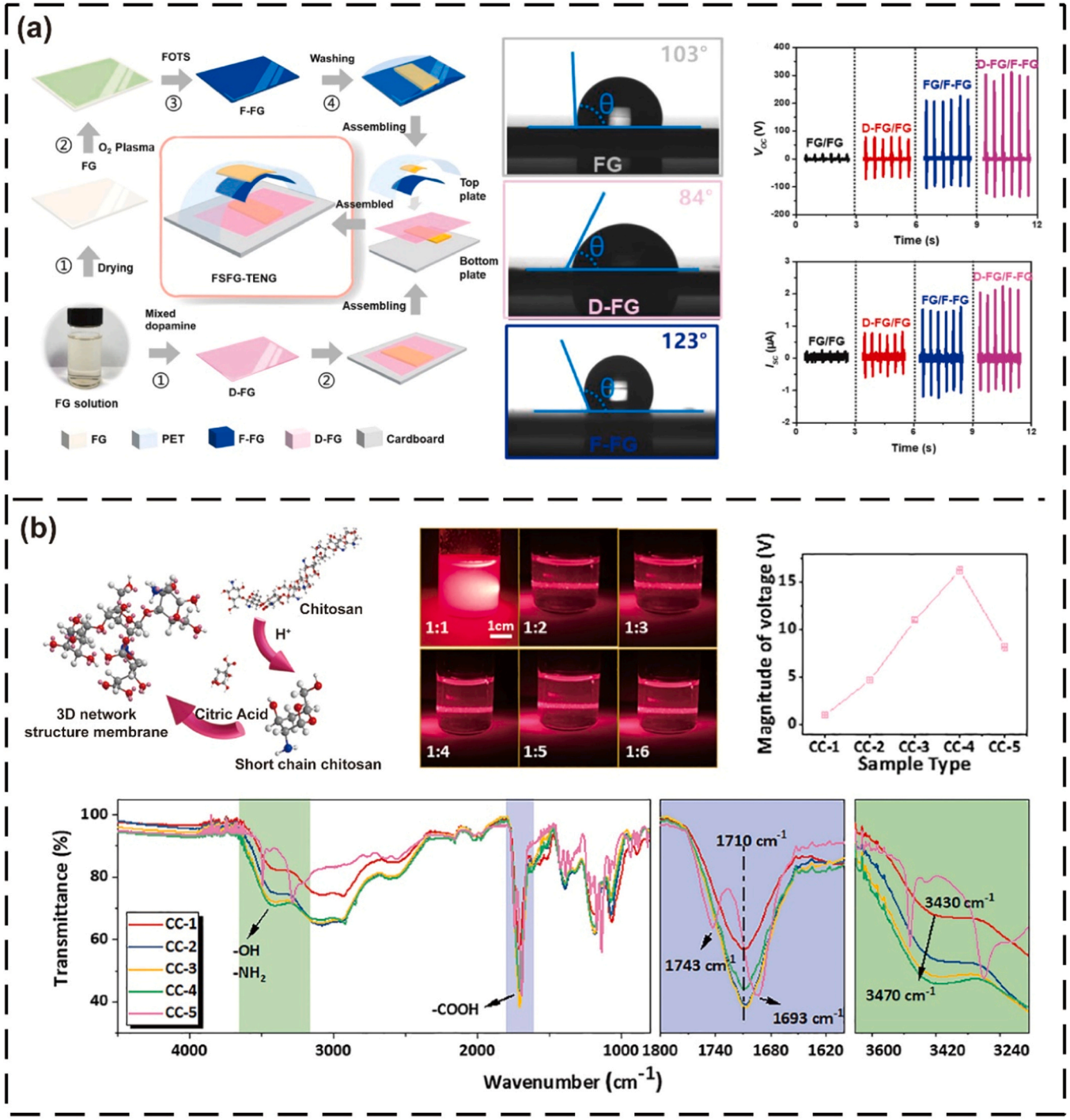

Fig. 9. Molecular surface engineering. (a) Preparation method and performance demonstration of a fish gelatin-based TENG that the two friction layers were modified with dopamine and fluorinated silane. Reproduced with permission. [113] Copyright 2021, Elsevier. (b) Facile molecular surface engineering in chitosan to improve the performance of chitosan-based TENG. Reproduced with permission. [121] Copyright 2019, Wiley-VCH.

alginate-metallic complexes can be primarily attributed to differences in their moisture absorption capabilities.

4.4. Molecular surface engineering

In addition to the above methods, chemical surface functionalization would be an effective method to enhance the TENG output performance. Some previous research studies have revealed that the chemical potential difference between the material surfaces has a great influence on the contact electrification, while the chemical potential is mainly determined by the electron affinity of their functional groups [117–119]. Thus, the surface potential of the tribo-materials could be adjusted by modifying various functional groups on the material surface for improving their triboelectric properties. For example, Liu et al. used the siloxane molecules self-assembly method to chemically modify the surface of cellulose nanofibrils with various functional groups (-CF_2CF_3, -CN, -SH, or -NH_2) [120]. The introduced -NH_2 and -SH functional groups make the modified cellulose nanofibrils more positive. However, -CN and -CF_2CF_3 functional groups tend to withdraw electrons, leading to modified cellulose nanofibrils with electronegativity.

Marine biomaterials contain abundant carboxyl groups (−COOH), amino (-NH_2), and hydroxyl (−OH) groups, which greatly improve their chemical modifiability for introducing strong electron donating or withdrawing groups. For instance, Sun et al. proposed a general method to develop a fish gelatin (FG)-based TENG, in which all tribo-materials were derived from discarded fish scales [113]. As shown in Fig. 9a, one FG film was doped with dopamine (denoted as D-FG), employed as the positive triboelectric layer. The another FG film was chemically grafted with trichloro(1H,1H,2H,2H-tridecafluoro-n-octyl)silane (FOTS) (denoted as F-FG), served as the negative triboelectric layer. The FG film was treated with oxygen plasma to hydroxylate its surface, followed by exposure to an atmosphere of FOTS at 40 ℃. During this processing step, target FOTS molecules were stuck to the surface of the FG film. This study employed water contact angle measurements to confirm the success of surface modification. The contact angles of the FG, D-FG, and F-FG films were 103°, 84°, and 123°, respectively, demonstrating that chemical modification can effectively tune the hydrophobic and hydrophilic properties of the surface. After chemical modification, the D-FG/F-FG paired TENG exhibited an outstanding electrical output performance, in which the voltage and current can reach 310 V and 2.5 μA. For comparison, the output voltage and current of the TENG with triboelectric pair of FG/FG were only 10 V and 0.2 μA, respectively.

Ma et al. introduced an alternative approach to effectively modulate the triboelectric polarity of chitosan (Fig. 9b) [121]. In their work, chitosan powder was dissolved in citric acid solution and hydrolyzed to short chain chitosan under acidic conditions. After that, a novel 3D network structure was created by hybridizing chitosan with citric acid, facilitated by the formation of hydrogen bonds and the cross-linking junction between the citric acid and chitosan fragmentation. The degree of hydrolysis can be verified by analyzing the Tyndall effect of the chitosan solution with mass ratios ranging from 1:2–1:6. Except for the sample with a 1:1 mass ratio, the Tyndall effect can be observed in other samples. The chitosan solutions with mass ratios from 1:2–1:6 (referred as CC-1 to CC-5) were used to fabricate chitosan film. Among these materials, the maximum voltage was ≈ 16.2 V, which was produced in CC-4. This result can be explained by analyzing the Fourier transform infrared spectroscopy, as shown in Fig. 9b. The band at 3430 cm^{-1} is attributed to the presence of exchangeable protons, which are closely related to hydroxyl groups and amino groups. From sample CC-1 to CC-4, the increasing of peak intensity indicates that more hydroxyl groups and amino groups are generated in the film. Since those groups are electron-donating groups, the corresponding surface electropositivity increases, leading to an improved triboelectric output performance.

4.5. Layer-by-layer assembly

The thickness of the triboelectric layer plays a crucial role in determining the output performance of TENGs. Generally, the thickness of those triboelectric layers is ranged from several ten micrometers to a few millimeters, which restricts their compatibility with future TENG applications. Layer-by-layer (LbL) assembly method is a novel technique for the fabrication of multilayer thin films with controllable thickness [122]. Menge et al. designed a high-performance ultrathin, and translucent chitosan (CH)-alginate (AL)-based TENG [123]. Protonated amine-rich CH solution is positively charged, while a carboxylate-rich AL solution is negatively charged so that CH-AL composites can be prepared by utilizing the strong electrostatic interaction. It is found that when the number of bilayers increase from 2 to 8, the output voltage increased from 180 V to 474 V. However, excessive number of bilayers widened the gap between the charge layer and conducting films, leading to a decrease in performance. In addition, the scanning Kelvin probe force microscopy (KPFM) method was applied to analyze the surface potential for a better understanding. The film composed of eight bilayers exhibited the highest surface potential of 239.4 mV, which is consistent with the previous experimental results.

5. Applications of marine biomaterial-based TENG

Due to high performance, biocompatibility, biodegradability, nontoxicity, and sustainability, marine biomaterial-based TENGs have been widely applied in many fields, ranging from energy harvesting to wearable self-powered active sensors. This section aims to present the latest developments in the utilization of marine biomaterial-based TENG reported in the literature.

5.1. Energy harvesting

Mechanical energy sources are ubiquitous in our living environment, such as wind, ocean waves, human movement, engine vibrations, and so on. Because of its advantages of high power density, lightweight, low cost, simplicity in manipulation, and environment-friendly, TENG is considered as a powerful and efficient approach for transforming mechanical energy into electric energy to power various types of electronic equipment. Han et al. fabricated a fish gelatin(FG) based triboelectric nanogenerator (FG-TENG) by pairing a FG film and PTFE/PDMS composite film (Fig. 10a) [124]. The authors demonstrated that the FG functioned as a superior tribo-material compared to the commonly utilized materials, exhibiting notably enhanced positive performance. Under periodic presses and releases, the fabricated TENG could easily light up 50 LEDs and charge a commercial capacitor to power an electronic calculator and electronic watch. Similarly, Saqib et al. proposed a TENG that used natural seagrass (Zostera marina and Phyllospadix japonicus) as positive tribo-material for the first time (Fig. 10b) [125]. Compared with the Zostera marina seagrass-based TENG, the Phyllospadix japonicus seagrass-based TENG has greater output performance, where the open circuit voltage, short circuit current, and maximum power density can reach about 288 V, 40 μA, and 70.42 $\mu W/cm^2$. With just a simple hand excitation force, the TENG demonstrates the ability to charge a commercial capacitor to drive low-power electronic devices.

Next generation of electronics will be soft, comfortable, and even biocompatible, and thus there is a pressing need for stretchable and sustainable power sources. Recently, stretchable TENGs have attracted intensive attention for their promising application in powering wearable electronics. For instance, Liu et al. prepared a stretchable TENG based on a PAAm-alginate hydrogel film as the electrode and polydimethylsiloxane (PDMS) as the electrification layer (Fig. 10c). This single electrode TENG has high transparent (90%) and stretchability (397%), making it an ideal candidate for seamlessly adhering to human skin to harness and convert human motion energies effectively. Furthermore, they also designed a contact−separation mode TENG,

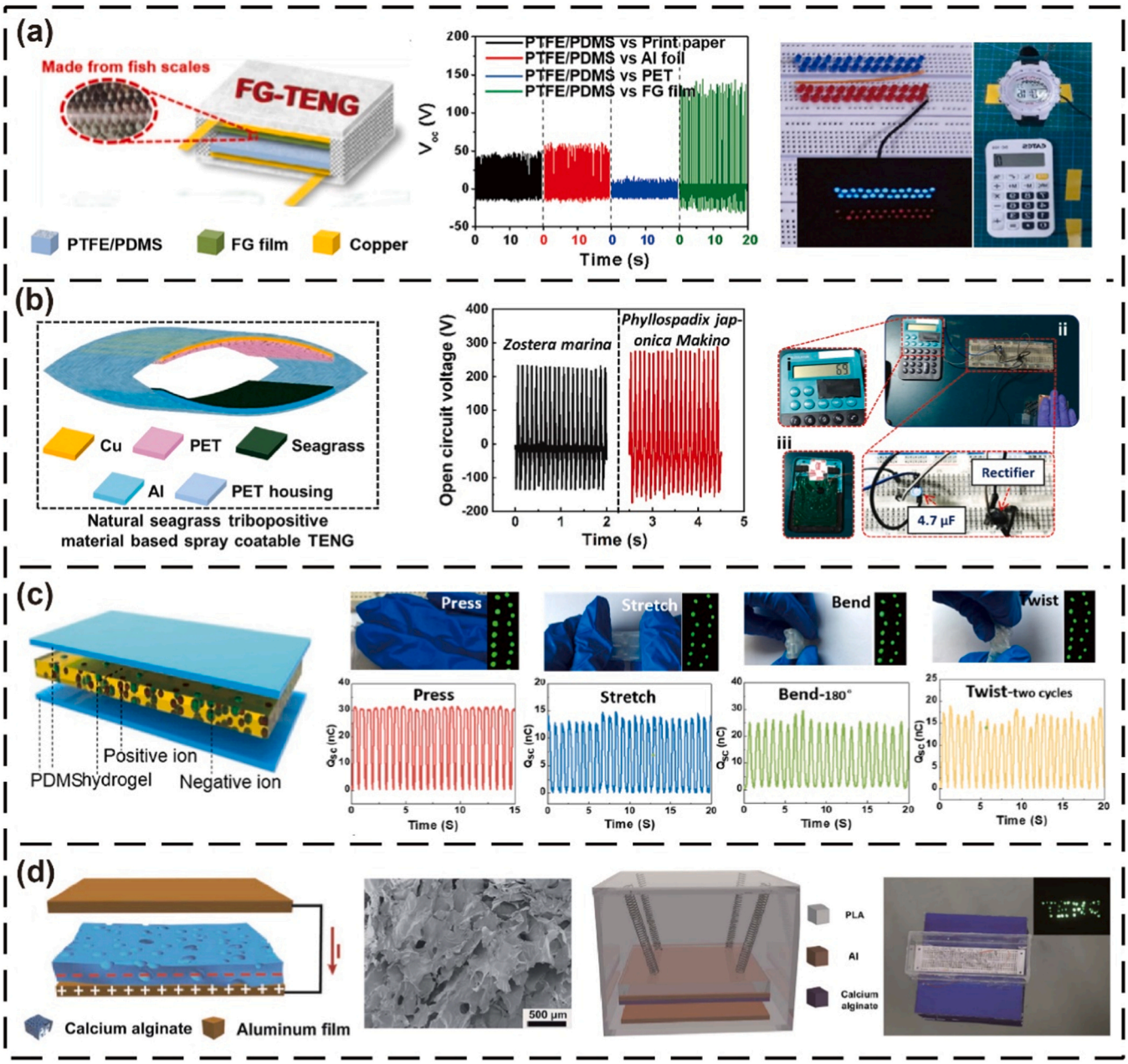

Fig. 10. Energy harvesting. (a) A fish gelatin(FG) based triboelectric nanogenerator (FG-TENG) by pairing a FG film and PTFE/PDMS composite film. Reproduced with permission. [124] Copyright 2020, American Chemical Society. (b) A TENG that used natural seagrass as positive tribo-material to drive electronic devices. Reproduced with permission. [125] Copyright 2021, Elsevier. (c) A stretchable TENG based on a PAAm-alginate hydrogel film as the electrode and PDMS as the electrification layer. Reproduced with permission. [160] Copyright 2018, American Chemical Society. (d) A degradable TENG built with alginate film for wave energy harvesting. Reproduced with permission. [129] Copyright 2018, Royal Society Of Chemistry.

which can harvest energy from an arbitrary mechanical movement to drive miniaturized electronics, such as pressing, stretching, bending, and twisting.

Ocean wave energy is a promising clean and renewable energy source for large-scale exploitation, with superior advantages of high-power density, wide distribution, and independence of time of day, weather or seasons. However, the exploitation of this energy is stagnating due to the limitation of inefficient energy harvesting technologies. As a newly developed technology, TENG has been proven to have impressive applications for ocean wave energy harvesting [126–128]. Our group reported a degradable TENG built with alginate film for wave energy harvesting (Fig. 10d) [129]. A calcium alginate film featuring porous structures was successfully produced using a simple freeze-drying technique combined with a crosslinking reaction. This film can rapidly degrade in the ocean environment without any pollution. For harvesting the irregular and ultra-low frequency wave energy, we designed a sealed degradable TENG composed of a polylactic acid (PLA) box, springs, and tribo-materials. Under the excitation of water waves, the two triboelectric layers contacted/separated, converting the wave energy to electrical energy to light up scores of LEDs. Nonetheless, further endeavors are imperative to design structures or modify materials to enhance the output performance and stability of the TENG in wave energy harvesting.

5.2. Smart textiles

The intersection of the growing appetite for wearable technologies and the advent of textile-based TENGs offers an exciting paradigm for the future of sustainable wearable devices. TENGs, celebrated for their efficient energy-harvesting capabilities, when amalgamated with the inherent properties of textiles—namely their flexibility, breathability, durability, and scalability—bring forth the next frontier in wearable innovations. Many groups have worked in developing smart textiles based on TENGs for energy harvesting and multifunctional self-powered sensing [130–133]. For instance, He et al. reported a self-powered fire alarm electronic textile (e-textile) based on sodium alginate [134]. Through wet-spinning, freeze-drying, and spray-coating, Fe_3O_4 nanoparticles and silver nanowires were introduced into sodium alginate-based aerogel fibers, which were further woven into electronic textiles (Fig. 11a). Owing to the interconnected three-dimensional porous network structure, the prepared e-textile can stand on the tip of the stamens, indicating the ultralight property of the device. The e-textile exhibited an ultrasensitive fire warning response with a wide temperature sensing range from 100° to 400°C. Such capabilities pave the way for its integration into the gear of firefighters. Once incorporated into their protective attire, this e-textile can continuously monitor surface temperatures, promptly raising alarms prior to the protective clothing succumbing to thermal breakdowns. Furthermore, the e-textile was used as a positive tribo-material to fabricate a textile-based TENG with excellent flexibility, which could be attached on different body parts to harvest human movement energy. It is noted that the prepared TENG can keep stable output performance even at 250 °C.

For textile-based electronics, washability and antibacterial properties are two important features for long-term use. Tian et al. reported

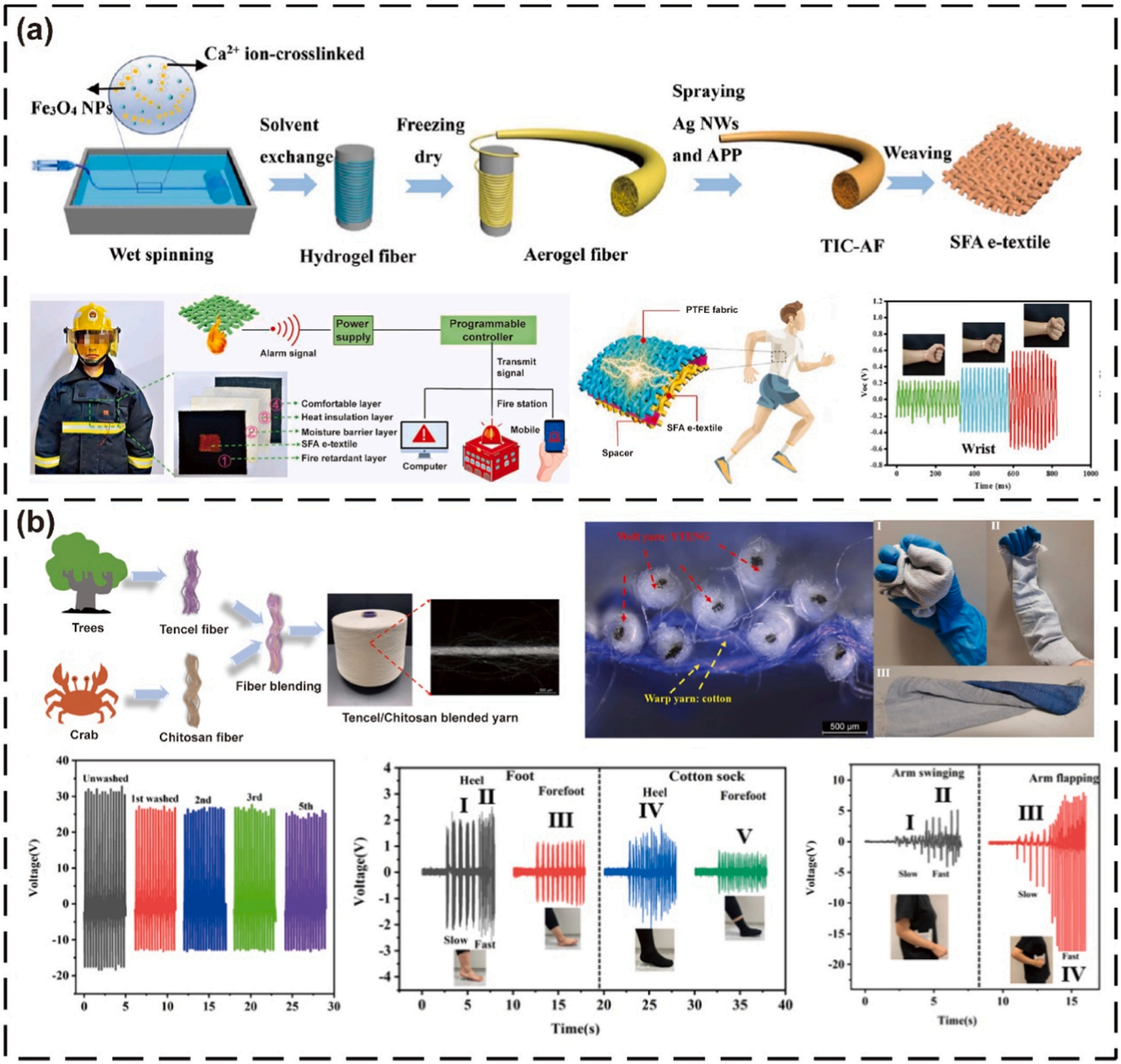

Fig. 11. Smart textiles. (a) The preparation and application of a self-powered fire alarm electronic textile based on sodium alginate. Reproduced with permission. [134] Copyright 2022, American Chemical Society. (b) Durable and antibacterial single-electrode triboelectric yarns composed of polyamide (PA) conductive yarns and Tencel/chitosan blended yarns. Reproduced with permission. [135] Copyright 2021, American Chemical Society.

durable and antibacterial single-electrode triboelectric yarns composed of polyamide (PA) conductive yarns and Tencel/chitosan blended yarns (Fig. 11b) [135]. Based on the existing weaving technology, a large, scaled textile TENG was fabricated by the continuously triboelectric yarns with high flexibility, small diameter, and low-cost. The output performance of the fabricated TENG showed small degradations after five washes, demonstrating the good machine washability of the device for daily use. Due to the presence of chitosan material and Ag coated on the PA yarn, the TENG exhibited excellent antibacterial properties. In addition, the TENG can be integrated on a sock or cloth to harvest energy and monitor body movement.

5.3. Self-powered multifunctional sensors

TENGs can be utilized as self-powered active mechanical sensors because they can transfer a stimulation/triggering into an electrical signal itself to respond to the input mechanical behaviors [136]. Kim et al. proposed a catechol-chitosan-diatom-based hydrogel conductor [137], which shows excellent stretchability and self-healing capability. With the help of a machine learning algorithm, they further developed a stretchable self-powered tremor sensor combining an M-shaped Kapton film with the hydrogel-based TENG for real-time monitoring of Parkinson's disease (PD) patients' health condition (Fig. 12a). Guo et al. reported a biocompatible and compliant triboelectric hydrogel sensor made from edible marine biomaterials for all-around infant motion

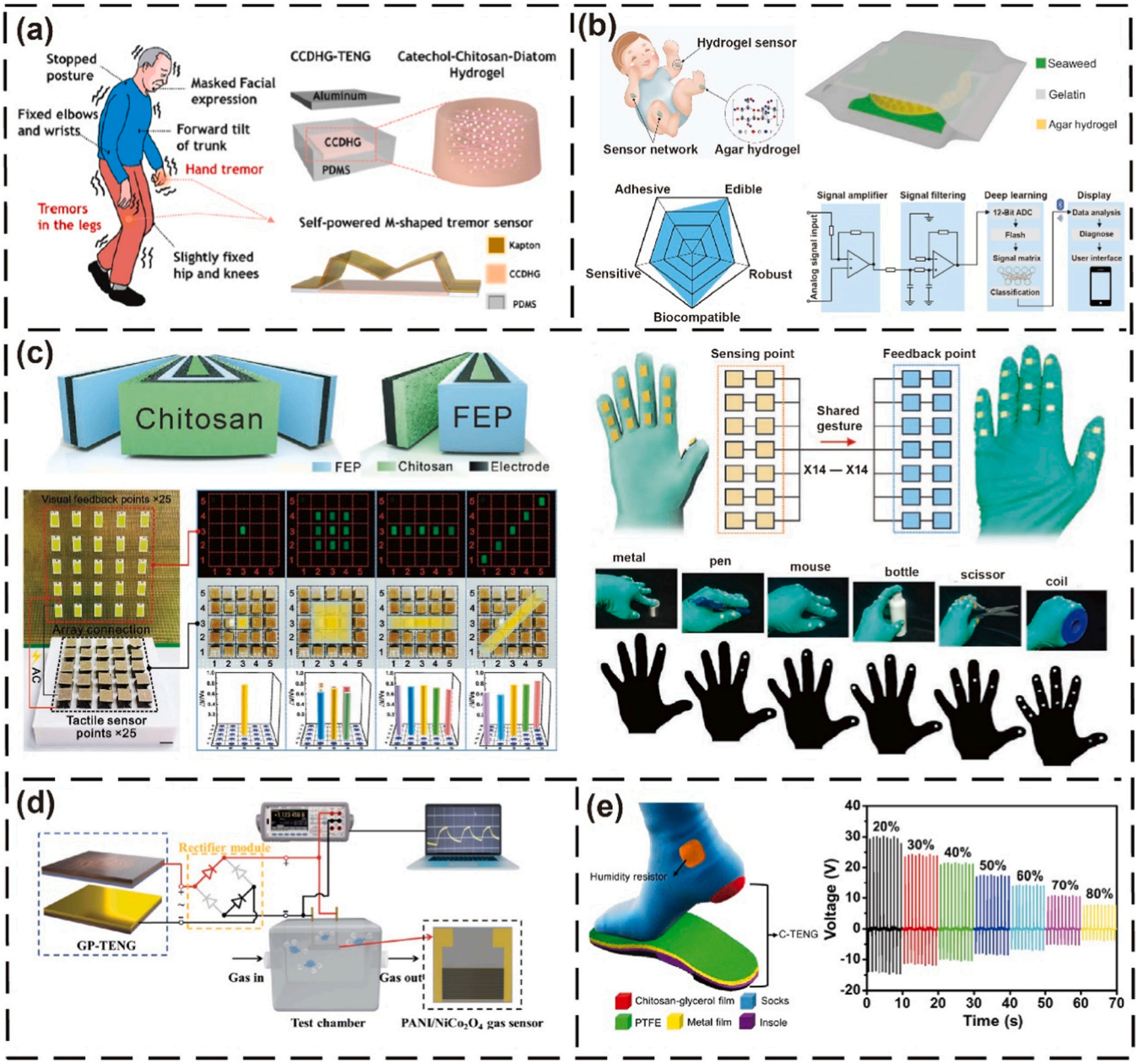

Fig. 12. Self-powered multifunctional sensors. (a) A stretchable self-powered tremor sensor. Reproduced with permission. [137] Copyright 2021, Elsevier. (b) A biocompatible and compliant triboelectric hydrogel sensor for infant motion monitoring. Reproduced with permission. [138] Copyright 2022, Wiley-VCH. (c) A wearable self-powered visual tactile sensor, which was composed of a chitosan-based X-shape TENG and a visual light source. Reproduced with permission. [139] Copyright 2023, Wiley-VCH. (d) A self-powered NH_3 gas sensor composed of the PANI/$NiCo_2O_4$ composite and gelatin/polyimide-based TENG. Reproduced with permission. [140] Copyright 2022, Royal Society Of Chemistry. (e) A self-powered humidity sensing system that consists of a chitosan-glycerol film-based humidity-sensitive resistor and a chitosan-based TENG integrated on a sock. Reproduced with permission. [141] Copyright 2018, Elsevier.

monitoring (Fig. 12b) [138]. The sensor showed a pressure sensitivity of about 0.28 V kPa^{-1}, a fast response time of 50 ms, and an impressive signal-to-noise ratio of 23.1 dB. The authors also proposed an infant care system, consisting of a sensor network, a signal-processing system, a deep learning algorithm system, and an APP display terminal. This system can promptly and accurately monitor the mechanical pressure applied to an infant's body and provide a real-time warning.

Recently, Lu et al. presented a wearable self-powered visual tactile sensor, which was composed of a chitosan-based X-shape TENG and a visual light source (Fig. 12c) [139]. With its remarkable output performance, the TENG can drive the LED through a mere touch and its luminous intensity showed a similar changing trend with that of applied load pressure. A 5 × 5 matrix was developed as an active tactile sensing system for remote visual tactile sensing. It was observed that the TENGs were able to produce stable output signals to power connected LEDs to provide visual feedback on pressure distribution. This study further developed a wearable palm state recognition system by assembling 14 sensors and corresponding LEDs on each finger joint to obtain motion-sensing information. As shown in Fig. 12c, different hand poses holding different objects could be easily recognized and classified by the visual feedback images.

According to the working principles of TENGs, the variation in the

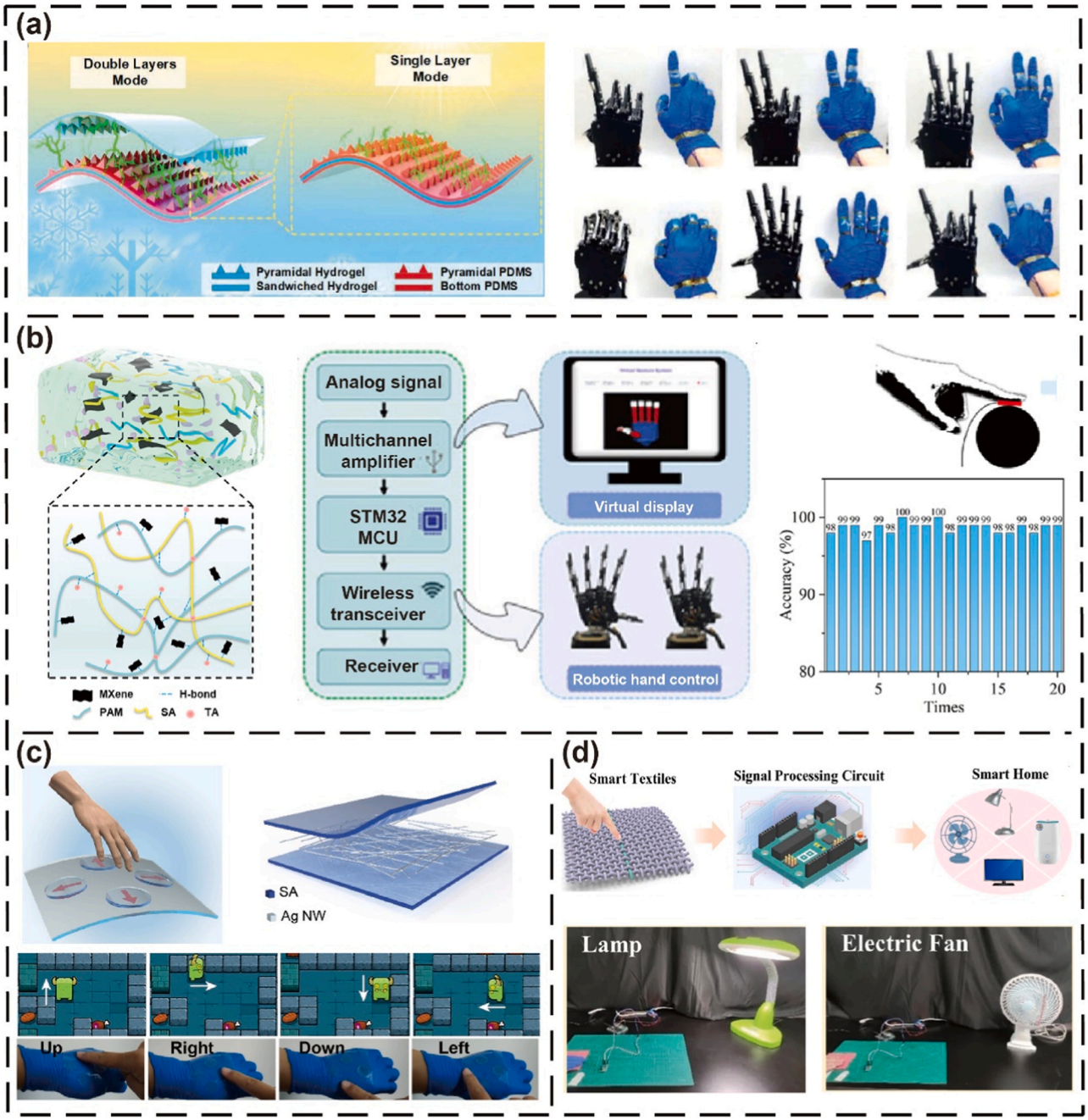

Fig. 13. Human-machine interfaces. (a) A TENG sensor based on micro-pyramid-patterned polyacrylamide/carrageenan DN hydrogel utilized to develop a self-powered HMI. Reproduced with permission. [161] Copyright 2022, Wiley-VCH. (b) An ionic hydrogel composed of polypropylene amine, tannic acid, sodium alginate and Mxene for robot hand control, object classification, and recognition. Reproduced with permission. [142] Copyright 2023, American Chemical Society. (c) A biodegradable, transparent, and antibacterial sodium alginate (SA)-based TENG array as the HMI for game control. Reproduced with permission. [143] Copyright 2023, Elsevier. (d) An HMI system for smart home applications by integrating a chitosan-based self-powered sensing fiber with a signal-processing circuit. Reproduced with permission. [144] Copyright 2022, American Chemical Society.

load sensor's resistance results in corresponding changes to the measured output amplitudes of the TENG. Therefore, except for sensing physical motion, TENGs also can be used to monitor the changes in the environment. Zhang et al. prepared a self-powered NH_3 gas sensor composed of the PANI/$NiCo_2O_4$ composite and gelatin/polyimide-based TENG (Fig. 12d) [140]. Integrated with a circuit module of rectification and voltage regulation, the TENG can generate a stable 24 V DC voltage signal to power the gas sensor. Results indicated that the output voltage of the TENG was positively correlated with the NH_3 concentration, and the sensor exhibited excellent repeatability, selectivity, and long-term stability. Jao et al. reported a self-powered humidity sensing system that consists of a chitosan-glycerol film-based humidity-sensitive resistor and a chitosan-based TENG integrated on a sock (Fig. 12e) [141]. The TENG on the foot can harvest mechanical energy and generates electric output flowing through the humidity sensor. The output voltage signal decreases with the increase of the relative humidity due to the enhancement of the conductivity of the chitosan-glycerol film.

5.4. Human-machine interface

Human-machine interface (HMI), as an emerging technology that can communicate and interact between humans and electric devices, has garnered significant attention in the field of smart homes, intelligent personal electronics, and biomedical instruments. In recent years, a variety of marine biomaterials-based TENGs have been used as self-powered human-machine interfaces since their output electric signal can serve as an input to control various electric devices. For instance, Tao et al. developed a TENG sensor based on micro-pyramid-patterned polyacrylamide (Paam)/carrageenan DN hydrogel utilized to develop a self-powered HMI (Fig. 13a). The device shows excellent flexibility, good transparency (≈85%), low limit of detection (50 Pa), high sensitivity (45.97 mV Pa^{-1}), and environmental tolerance (−20 to 60 °C). By designing the signal acquisition/process circuit, the TENG sensor can be used as a switching button and a self-powered HMI for robot hand control. With the bending of the TENG sensor fastened on a finger, a voltage pulse is generated and used as a trigger signal to control the robot hand's actions, imitating the movements of the operator's hand. More ingeniously, Zhang et al. also demonstrated the capability for human-machine interaction of a marine biomaterials-based TENG [142]. They prepared an ionic hydrogel (PTSM) composed of polypropylene amine (PAM), tannic acid (TA), sodium alginate (SA), and MXene, with remarkable stretchability (strain>4600%), impressive adhesion, and good self-healing ability (Fig. 13b). Based on the PTSM and microcontrollers, a glove-based HMI system was constructed with the functions of gesture visualization and wireless robot hand control. With the help of machine learning algorithm, the device can achieve object classification and recognition with recognition accuracy of 97–100%.

In addition to the mentioned application scenarios, the marine biomaterial-based TENG has also demonstrated its applications in wearable self-powered control systems. For example, Li et al. reported a biodegradable, transparent, and antibacterial sodium alginate (SA)-based TENG array as the HMI for game control (Fig. 13c) [143]. Four TENG sensing units as the function keys were connected to a laptop through an Arduino microcontroller. Once the unit was touched by a human finger, a voltage signal was generated to control the movement of the character in the gaming interface. In another example, Li et al. developed an HMI system for smart home applications by integrating a chitosan-based self-powered sensing fiber with a signal-processing circuit [144] (Fig. 13d). They prepared chitosan from the waste material and then fabricated sensing fiber by electrospinning core wire technique. In their study, a touch pressure was captured by the TENG sensing fiber and the generated electric signal was converted into digital signals by the microcontroller unit to control household appliances, such as a table lamp and a fan.

5.5. Fully biodegradable transient electronics

The surging consumption of electronic gadgets has exponentially increased e-waste, casting severe ecological challenges. An ingenious approach to tackle this concern is through transient technology—electronics designed to gracefully degrade into the environment after a designated duration, leaving negligible traces or harm [145,146]. In this realm, marine biomaterials, credited for their abundant availability, biocompatibility, and impeccable biodegradability, have emerged as a stellar choice for crafting transient energy harvesters. For instance, Liang et al. designed a recyclable and green TENG (Fig. 14a), consisting of surface-patterned polyvinyl alcohol (PVA) and SA as tribo-materials, lithium (Li) and aluminum (Al) as electrode materials [147]. All the components of the device could completely degrade in water within 10 min, based on their excellent solubility and cascade chemical reactions without releasing any toxic substances. More importantly, the generated solution from the dissolution process can be reused to fabricate a new TENG device with no waste and environmental pollution, and the new device showed output performance comparable to the original TENG device.

Similarly, gelatin was also applied for biodegradable tribo-materials. Pan et al. reported a fully biodegradable TENG device built with degradable metal Mg, nanostructured gelatin films, and electrospun polylactic acid (PLA) (Fig. 14b) [148]. By optimizing the surface morphology of the two triboelectric layers, the TENG achieves an impressive output voltage of approximately 900 V and a power density over 5 W/cm^2. As shown in Fig. 14b, the Mg electrode of 100 μm can dissolve almost completely in water over 18 days, while the Mg/gelatin and MG/PLA can completely degrade in about 20 days. Recently, Peng et al. fabricated a flexible, transparent, and biodegradable e-skin by using CS films as both the triboelectric layer and substrate, along with Au nanofibers serving as the intermediate electrode. (Fig. 14c) [149]. Because CS is formed of 2-acetamido-d-glucose and 2-amino-d-glucose linked by glycosidic linkages, it is easily destroyed and degraded into oligomers. The device's biodegradability was assessed by immersing it in various media, such as acetic acid solution, hydrogen peroxide solution, and pepsin solution. It is observed that the device quickly swelled, and totally degraded after 30 h.

6. Conclusions and perspectives

Marine biomaterials, abundant renewable treasures from the oceans, possess unique attributes that make them ideal for TENG device fabrication, including cost-effectiveness, vast availability, superior biocompatibility, exceptional biodegradability, and safety. Consequently, there has been a burgeoning interest in marine biomaterial-derived TENGs, spotlighting their vast potential for real-world applications. In this review, we examine the evolution of these marine biomaterial-based TENGs, from fundamental concepts to tangible applications. We initiate with an understanding of the TENG's operational mechanism, laying the foundation for its marine biomaterial-driven variants. Subsequently, we delve into the intrinsic properties of frequently employed marine biomaterials, elucidate strategies to enhance the performance of these TENGs, and highlight their promising applications. Given the ongoing deep dives into materials and structural designs, we are optimistic about significant strides in the development and extensive applications of marine biomaterial-centric TENGs. However, several challenges await resolution before their commercial deployment (Fig. 15).

First, the output energy of the marine biomaterial-based TENGs should be further improved to meet the demand for a continuous power supply of electronics. As shown in Table 1, the majority of marine biomaterial-based TENGs have relatively low output performance that severely impedes the practical application of TENGs. Generally, marine biomaterials are used as positive tribo-materials due to the existence of widely distributed electron-donating groups. Although there have been

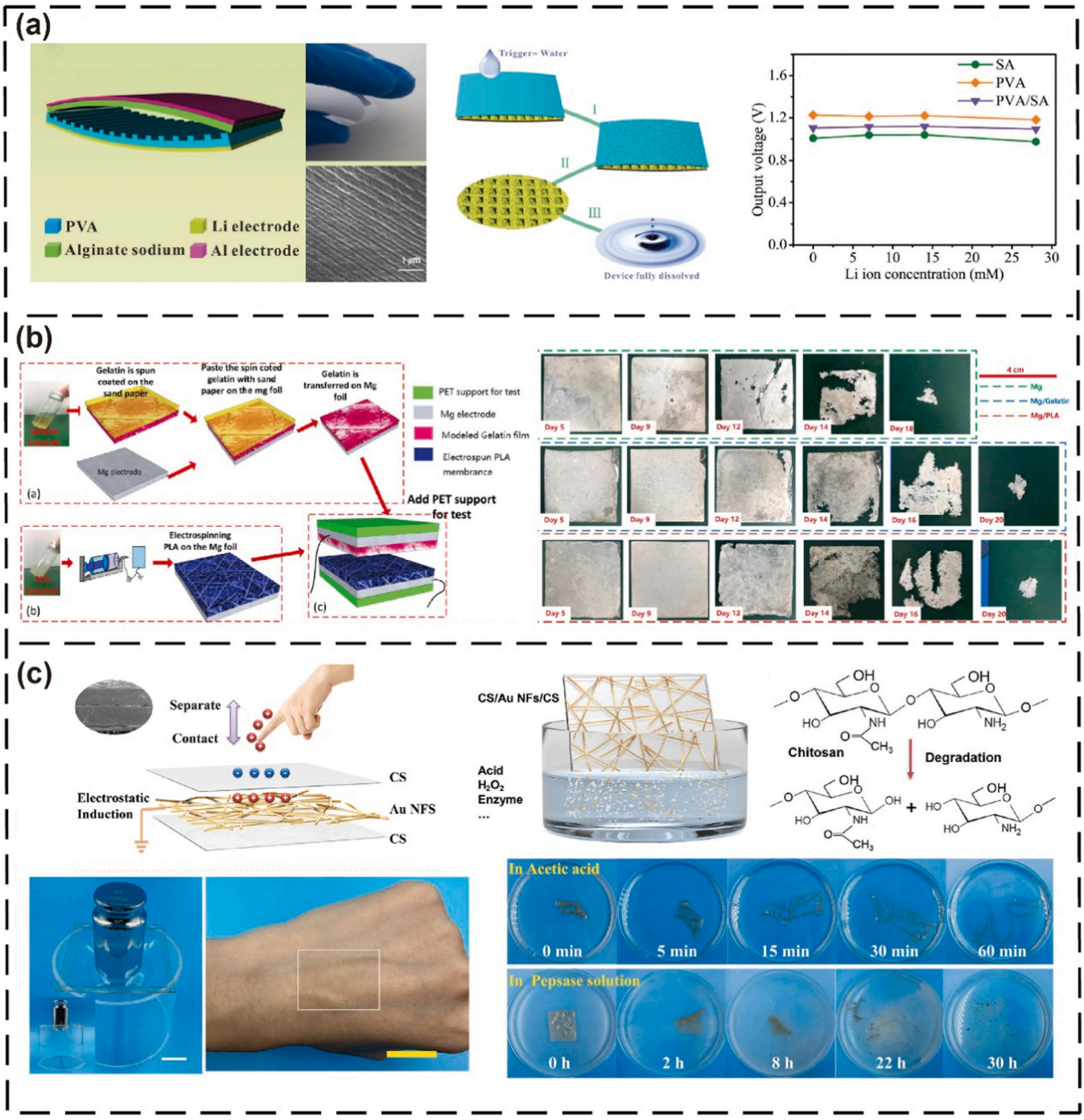

Fig. 14. Fully biodegradable transient electronics. (a) A recyclable and green TENG, consisting of surface-patterned polyvinyl alcohol and sodium alginate as tribo-materials, lithium and aluminum as electrode materials. Reproduced with permission. [147] Copyright 2017, Wiley-VCH. (b) A fully biodegradable TENG device built with degradable metal Mg, nanostructured gelatin films, and electrospun polylactic acid. Reproduced with permission. [148] Copyright 2018, Elsevier. (c) A flexible, transparent, and biodegradable e-skin by using chitosan films as both the triboelectric layer and substrate, along with Au nanofibers serving as the intermediate electrode. Reproduced with permission. [149] Copyright 2022, American Chemical Society.

some studies in which marine biomaterials were modified by chemical/physical methods to increase the electron-withdrawing ability, there exist great gaps between marine biomaterials and traditional negative tribo-materials, such as PTFE and polyimide. In future research, it is necessary to invent and improve new strategies for optimizing power generation performance, such as creating micro-/nanostructures, high-voltage charge injection, and designing innovative structures. Some marine biomaterials contain abundant carboxyl groups (−COOH) and hydroxyl (−OH) groups, which greatly improves their chemical modifiability for introducing strong electron donating or withdrawing groups [150].

Second, the mechanical stability and durability of materials and devices are required to be improved because it is crucial for the long-term operations of TENGs. Most marine biomaterials have good water solubility, while humidity has a negative impact on the output performance of TENG which restricts their applications in humid environments. For wearable smart textiles, washability is a basic requirement for long-term use. Therefore, it is vital to develop high-performance

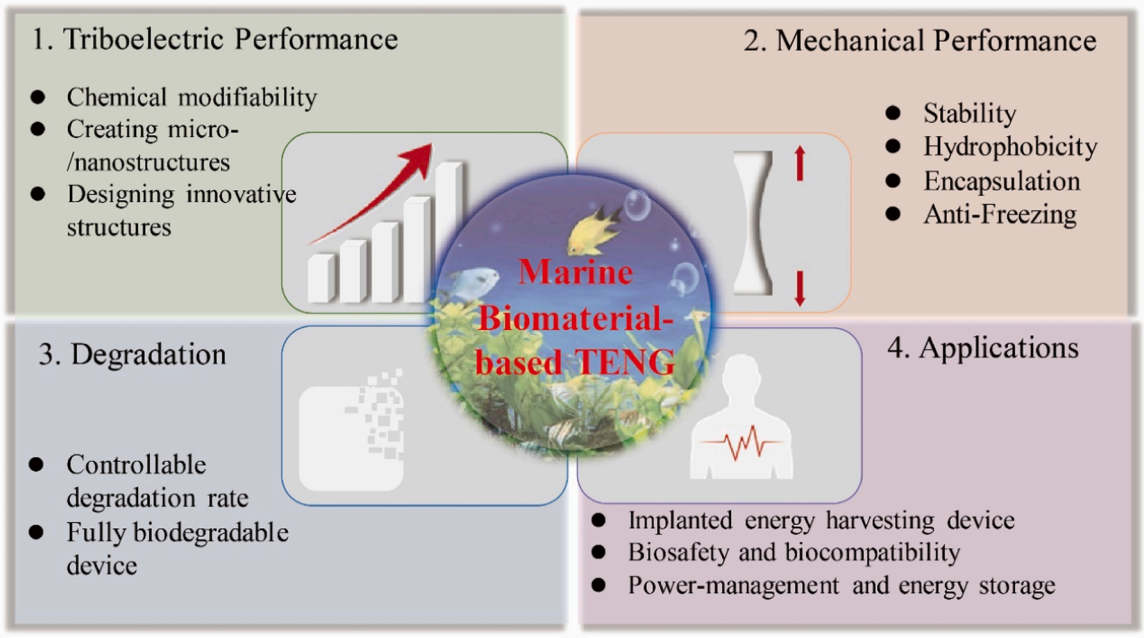

Fig. 15. Future challenges and prospects of marine biomaterial-based TENGs.

waterproof encapsulating materials or anti-humidity technologies to protect devices from harsh working environments. In addition to tribomaterials, marine biomaterials are widely used as an important component of conductive hydrogel electrodes in TENGs. The mechanical and conductive properties of the hydrogel will inevitably decline with loss of water under dryness and freeze under subzero temperatures. Changing solvent, introducing hydrated salts, and encapsulation with elastomers are some potential strategies available to address these issues [151–153].

Third, marine biomaterials are beneficial polymers for eco-friendly TENGs due to their excellent degradability. Currently, marine biomaterials just replace certain partial components of the entire devices, and there has been very little research in fully biodegradable marine biomaterial-based TENGs. The degradation rate of the devices is important for their utilization. Too fast degradation will lead to shorter service time that cannot meet the application requirements, while too slow degradation may cause problems for the environment. Therefore, the controllable degradation rate of TENGs will be essential for their practical applications in energy, wearable electronics, and biomedicine, and more research attention should be given to developing new methods through physical, biological, and chemical stimulation to control degradation.

Fourth, the application scope of marine biomaterial-based TENG should be further expanded. Although various marine biomaterial-based TENGs have been developed and could generate good electrical output, their applications are mainly confined to basic applications, such as lighting up the LEDs, powering electronic watches, and the self-powered pressure sensor. To further promote their commercialization process and reflect on their advantages, more efforts are required to explore new applications. For example, marine biomaterial has the unique properties of biocompatibility, biodegradability, and nontoxicity of marine biomaterials, which make it suitable for developing implanted TENGs to realize in vivo biomedical monitoring and energy harvesting. Significantly, all components of implanted TENG, including triboelectric layers, encapsulation layers, substrate layers, and electrodes, should meet the biosafety and biocompatibility requirements. Moreover, with researchers' continuous efforts, various wearable TENGs are designed to harvest biomechanical energy or used as electronic skins. Considering that most wearable TENGs are in direct contact with human skin, further investigations related to antibacterial characteristics, breathability, and flexibility of the device should be devoted to meeting the usage requirement of electronic skin. Finally, to improve the applicability and practicability of TENG, it is necessary to develop highly efficient power-management circuits and energy storage devices [154,155].

CRediT authorship contribution statement

Yunmeng Li: Investigation, Conceptualization, Methodology, Data curation, Visualization, Writing – original draft. **Xin Liu**: Investigation, Conceptualization, Methodology, Data curation. **Zewei Ren**: Data curation, Visualization. **Jianjun Luo**: Data curation, Visualization. **Chi Zhang**: Writing – review & editing. **Changyong (Chase) Cao:** Writing – review & editing. **Hua Yuan**: Supervision. **Yaokun Pang:** Supervision.

Declaration of Competing Interest

The authors declare that they have no known competing financial interests or personal relationships that could have appeared to influence the work reported in this paper.

Data availability

Data will be made available on request.

Acknowledgments

This work was partially supported by the National Natural Science Foundation of China (Grant 52203315), Natural Science Foundation of Shandong Province (ZR2022QE007, ZR2021JQ16, ZR2019YQ19), Excellent Youth Science Fund Project (Overseas) of Shandong Province (2023HWYQ-088), State Key Laboratory for Modification of Chemical Fibers and Polymer Materials (KF2301).

References

[1] S.J. Sarma, S.K. Brar, E.B. Sydney, Y. Le Bihan, G. Buelna, C.R. Soccol, Int. J. Hydrog. Energy 37 (2012) 6473–6490.
[2] D. Gielen, F. Boshell, D. Saygin, M.D. Bazilian, N. Wagner, R. Gorini, Energy Strategy Rev. 24 (2019) 38–50.
[3] R.M. Elavarasan, Eur. J. Sustain. Dev. Res. 3 (2019) em0076.
[4] Z. Wu, T. Cheng, Z.L. Wang, Sensors 20 (2020) 2925.

[5] R. Hidalgo-Leon, J. Urquizo, C.E. Silva, J. Silva-Leon, J. Wu, P. Singh, G. Soriano, Energy Rep. 8 (2022) 3809–3826.
[6] Z. Ren, L. Wu, Y. Pang, W. Zhang, R. Yang, Nano Energy 100 (2022), 107522.
[7] W.G.P. Kumari, P.G. Ranjith, Earth-Sci. Rev. 199 (2019), 102955.
[8] Y. Rong, Y. Hu, A. Mei, H. Tan, M.I. Saidaminov, S.I. Seok, M.D. McGehee, E. H. Sargent, H. Han, Science 361 (2018), eaat8235.
[9] M. Zhou, M.S.H. Al-Furjan, J. Zou, W. Liu, Renew. Sustain. Energy Rev. 82 (2018) 3582–3609.
[10] F.-R. Fan, Z.-Q. Tian, Z. Lin Wang, Nano Energy 1 (2012) 328–334.
[11] Z.L. Wang, Faraday Discuss. 176 (2014) 447–458.
[12] C. Zhang, W. Tang, C. Han, F. Fan, Z.L. Wang, Adv. Mater. 26 (2014) 3580–3591.
[13] W. Wang, W. Sun, Y. Du, W. Zhao, L. Liu, Y. Sun, D. Kong, H. Xiang, X. Wang, Z. Li, Q. Ma, ACS Nano 17 (2023) 9793–9825.
[14] Y. Lu, L. Jiang, Y. Yu, D. Wang, W. Sun, Y. Liu, J. Yu, J. Zhang, K. Wang, H. Hu, X. Wang, Q. Ma, X. Wang, Nat. Commun. 13 (2022) 5316.
[15] X. Li, T.H. Lau, D. Guan, Y. Zi, J. Mater. Chem. A 7 (2019) 19485–19494.
[16] Y. Zheng, T. Liu, J. Wu, T. Xu, X. Wang, X. Han, H. Cui, X. Xu, C. Pan, X. Li, Adv. Mater. 34 (2022), e2202238.
[17] W. Shang, G. Gu, W. Zhang, H. Luo, T. Wang, B. Zhang, J. Guo, P. Cui, F. Yang, G. Cheng, Z. Du, Nano Energy 82 (2021), 105725.
[18] Y. Pang, S. Chen, J. An, K. Wang, Y. Deng, A. Benard, N. Lajnef, C. Cao, Adv. Funct. Mater. 30 (2020), 2003598.
[19] C. Xu, X. Fu, C. Li, G. Liu, Y. Gao, Y. Qi, T. Bu, Y. Chen, Z.L. Wang, C. Zhang, Microsyst. Nanoeng. 8 (2022) 30.
[20] Y. Pang, Y. Fang, J. Su, H. Wang, Y. Tan, C. Cao, Adv. Mater. Technol. (2023) 2201246.
[21] Y. Pang, S. Chen, Y. Chu, Z.L. Wang, C. Cao, Nano Energy 66 (2019), 104131.
[22] X. Guo, J. He, Y. Zheng, J. Wu, C. Pan, Y. Zi, H. Cui, X. Li, Nano Res. Energy 2 (2023), e9120074.
[23] X. Pu, C. Zhang, Z.L. Wang, Natl. Sci. Rev. 10 (2023), nwac170.
[24] Z. Zhang, G. Gu, Y. Liu, J. Wang, G. Gu, W. Zhang, G. Cheng, Z. Du, Adv. Eng. Mater. (2022) 2201273.
[25] W. Li, L. Lu, A.G.P. Kottapalli, Y. Pei, Nano Energy 95 (2022), 107018.
[26] Y. Pang, S. Chen, Y. Cao, Z. Huang, X. Xu, Y. Fang, C. Cao, Adv. Mater. Interfaces 9 (2022), 2201202.
[27] J. Wang, P. Cui, J. Zhang, Y. Ge, X. Liu, N. Xuan, G. Gu, G. Cheng, Z. Du, Nano Energy 89 (2021), 106320.
[28] J. Luo, Z. Wang, L. Xu, A.C. Wang, K. Han, T. Jiang, Q. Lai, Y. Bai, W. Tang, F. R. Fan, Z.L. Wang, Nat. Commun. 10 (2019) 5147.
[29] M. Haghayegh, R. Cao, F. Zabihi, R. Bagherzadeh, S. Yang, M. Zhu, J. Mater. Chem. C 10 (2022) 11439–11471.
[30] Z. Su, Y. Yang, Q. Huang, R. Chen, W. Ge, Z. Fang, F. Huang, X. Wang, Prog. Mater. Sci. 125 (2022), 100917.
[31] H. Yang, F.R. Fan, Y. Xi, W. Wu, Adv. Sustain. Syst. 4 (2020), 2000108.
[32] F.G. Torres, G.E. De-la-Torre, Carbohydr. Polym. 251 (2021), 117055.
[33] X. Li, C. Jiang, Y. Ying, J. Ping, Adv. Energy Mater. 10 (2020), 2002001.
[34] P. Manivasagan, S. Bharathiraja, M.S. Moorthy, Y.-O. Oh, H. Seo, J. Oh, Polym. Rev. 57 (2017) 631–667.
[35] Y. Khrunyk, S. Lach, I. Petrenko, H. Ehrlich, Mar. Drugs 18 (2020) 589.
[36] H. Zhang, X. Wu, L. Quan, Q. Ao, Mar. Drugs 20 (2022) 372.
[37] P. Manivasagan, J. Oh, Int. J. Biol. Macromol. 82 (2016) 315–327.
[38] P. Laurienzo, Mar. Drugs 8 (2010) 2435–2465.
[39] X. Jing, Y. Sun, X. Ma, H. Hu, Mater. Chem. Front. 5 (2021) 5595–5616.
[40] H. Wang, Q. An, Z. Xiao, Y. Tong, L. Guo, S. Zhai, L.-P. Xiao, C.-S. Ha, J. Mater. Chem. A 10 (2022) 17023–17052.
[41] L. Valentini, N. Rescignano, D. Puglia, M. Cardinali, J. Kenny, Eur. J. Inorg. Chem. 2015 (2014) 1192–1197.
[42] S. Chao, H. Ouyang, D. Jiang, Y. Fan, Z. Li, EcoMat 3 (2020), e12072.
[43] J. Lowell, A.C. Rose-Innes, Adv. Phys. 29 (1980) 947–1023.
[44] Z.L. Wang, A.C. Wang, Mater. Today 30 (2019) 34–51.
[45] C. Xu, Y. Zi, A.C. Wang, H. Zou, Y. Dai, X. He, P. Wang, Y.C. Wang, P. Feng, D. Li, Z.L. Wang, Adv. Mater. 30 (2018), e1706790.
[46] Z.L. Wang, Mater. Today 20 (2017) 74–82.
[47] Z.L. Wang, Nano Energy 68 (2020), 104272.
[48] Z.L. Wang, Mater. Today 52 (2022) 348–363.
[49] J. Luo, Z.L. Wang, EcoMat 2 (2020), e12059.
[50] W. Akram, Q. Chen, G. Xia, J. Fang, Nano Energy 106 (2023), 108043.
[51] R. Abka-Khajouei, L. Tounsi, N. Shahabi, A.K. Patel, S. Abdelkafi, P. Michaud, Mar. Drugs 20 (2022) 364.
[52] K. Teng, Q. An, Y. Chen, Y. Zhang, Y. Zhao, ACS Biomater. Sci. Eng. 7 (2021) 1302–1337.
[53] D. Bi, X. Yang, L. Yao, Z. Hu, H. Li, X. Xu, J. Lu, Mar. Drugs 20 (2022) 564.
[54] C. Lacoste, R. El Hage, A. Bergeret, S. Corn, P. Lacroix, Carbohydr. Polym. 184 (2018) 1–8.
[55] K.Y. Lee, D.J. Mooney, Prog. Polym. Sci. 37 (2012) 106–126.
[56] S. Saji, A. Hebden, P. Goswami, C. Du, Sustainability 14 (2022) 5181.
[57] J.-S. Yang, Y.-J. Xie, W. He, Carbohydr. Polym. 84 (2011) 33–39.
[58] M. Urbanova, M. Pavelkova, J. Czernek, K. Kubova, J. Vyslouzil, A. Pechova, D. Molinkova, J. Vyslouzil, D. Vetchy, J. Brus, Biomacromolecules 20 (2019) 4158–4170.
[59] E.V.R. Campos, J.L. Oliveira, L.F. Fraceto, Front. Chem. 5 (2017), 93.
[60] H. El Knidri, R. Belaabed, A. Addaou, A. Laajeb, A. Lahsini, Int. J. Biol. Macromol. 120 (2018) 1181–1189.
[61] I. Younes, M. Rinaudo, Mar. Drugs 13 (2015) 1133–1174.
[62] J. Li, S. Zhuang, Eur. Polym. J. 138 (2020), 109984.
[63] P. Singh, R. Nagendran, Appl. Water Sci. 6 (2014) 199–204.
[64] J. Zhang, Y. Hu, X. Lin, X. Qian, L. Zhang, J. Zhou, A. Lu, Carbohydr. Polym. 291 (2022), 119586.
[65] Z.A. Nur Hanani, Y.H. Roos, J.P. Kerry, Int. J. Biol. Macromol. 71 (2014) 94–102.
[66] A.A. Karim, R. Bhat, Food Hydrocoll. 23 (2009) 563–576.
[67] L. Lin, J.M. Regenstein, S. Lv, J. Lu, S. Jiang, Trends Food Sci. Technol. 68 (2017) 102–112.
[68] P. Guerrero, P.M. Stefani, R.A. Ruseckaite, K. de la Caba, J. Food Eng. 105 (2011) 65–72.
[69] L.-C. Lv, Q.-Y. Huang, W. Ding, X.-H. Xiao, H.-Y. Zhang, L.-X. Xiong, J. Funct. Foods 63 (2019), 103581.
[70] P. Aramwit, N. Jaichawa, J. Ratanavaraporn, T. Srichana, Mater. Express 5 (2015) 241–248.
[71] G. Sharma, A. Khosla, A. Kumar, N. Kaushal, S. Sharma, M. Naushad, D.N. Vo, J. Iqbal, F.J. Stadler, Chemosphere 289 (2022), 133100.
[72] S.A. Qamar, M. Junaid, A. Riasat, M. Jahangeer, M. Bilal, B.Z. Mu, Starch (2022) 2200018.
[73] L. Li, R. Ni, Y. Shao, S. Mao, Carbohydr. Polym. 103 (2014) 1–11.
[74] V.L. Campo, D.F. Kawano, D.B. d Silva, I. Carvalho, Carbohydr. Polym. 77 (2009) 167–180.
[75] S. Liu, S. Huang, L. Li, J. Rheol. 60 (2016) 203–214.
[76] S. Kara, E. Arda, B. Kavzak, Ö. Pekcan, J. Appl. Polym. Sci. 102 (2006) 3008–3016.
[77] S.R. Derkach, N.G. Voron'ko, Y.A. Kuchina, D.S. Kolotova, A.M. Gordeeva, D. A. Faizullin, Y.A. Gusev, Y.F. Zuev, O.N. Makshakova, Carbohydr. Polym. 197 (2018) 66–74.
[78] Y. Dong, Z. Wei, C. Xue, Trends Food Sci. Technol. 112 (2021) 348–361.
[79] A. Jafari, M. Farahani, M. Sedighi, N. Rabiee, H. Savoji, Carbohydr. Polym. 281 (2022), 119045.
[80] J.P. Serra, N. Pereira, D.M. Correia, C.R. Tubio, J.L. Vilas-Vilela, C.M. Costa, S. Lanceros-Mendez, ACS Sustain. Chem. Eng. 10 (2022) 8631–8640.
[81] J. Liu, X. Zhan, J. Wan, Y. Wang, C. Wang, Carbohydr. Polym. 121 (2015) 27–36.
[82] Z. Noralian, M.P. Gashti, M.R. Moghaddam, H. Tayyeb, I. Erfanian, Int. J. Biol. Macromol. 180 (2021) 439–457.
[83] Z. Chen, J. Yu, H. Zeng, Z. Chen, K. Tao, J. Wu, Y. Li, Micromachines 12 (2021) 1462.
[84] Y. Wu, Y. Luo, T.J. Cuthbert, A.V. Shokurov, P.K. Chu, S.P. Feng, C. Menon, Adv. Sci. 9 (2022), e2106008.
[85] F.G. Torres, O.P. Troncoso, G.E. De-la-Torre, Int. J. Energy Res. 46 (2021) 5603–5624.
[86] T. Zhu, Y. Ni, G.M. Biesold, Y. Cheng, M. Ge, H. Li, J. Huang, Z. Lin, Y. Lai, Chem. Soc. Rev. 52 (2023) 473–509.
[87] X. Jing, H. Li, H.Y. Mi, P.Y. Feng, X. Tao, Y. Liu, C. Liu, C. Shen, ACS Appl. Mater. Interfaces 12 (2020) 23474–23483.
[88] X. Li, S. Xiang, D. Ling, S. Zhang, C. Li, R. Dai, P. Zhu, X. Liu, Z. Pan, Mater. Sci. Eng. B 283 (2022), 115832.
[89] H. Sun, Y. Zhao, S. Jiao, C. Wang, Y. Jia, K. Dai, G. Zheng, C. Liu, P. Wan, C. Shen, Adv. Funct. Mater. 31 (2021), 2101696.
[90] B. Ying, R. Zuo, Y. Wan, X. Liu, ACS Appl. Electron. Mater. 4 (2022) 1930–1938.
[91] M. Wu, X. Wang, Y. Xia, Y. Zhu, S. Zhu, C. Jia, W. Guo, Q. Li, Z. Yan, Nano Energy 95 (2022).
[92] L. Wang, W.A. Daoud, Nano Energy 66 (2019), 104080.
[93] Q.-M. Huang, H. Yang, S. Wang, X. Liu, C. Tan, A. Luo, S. Xu, G. Zhang, H. Ye, ACS Appl. Nano Mater. 6 (2023) 10453–10465.
[94] Y. Liu, Y. Shen, W. Ding, X. Zhang, W. Tian, S. Yang, B. Hui, K. Zhang, npj Flex. Electron. 7 (2023), 21.
[95] J.-N. Kim, J. Lee, T.W. Go, A. Rajabi-Abhari, M. Mahato, J.Y. Park, H. Lee, I.-K. Oh, Nano Energy 75 (2020), 104904.
[96] J. Chen, H. Guo, X. He, G. Liu, Y. Xi, H. Shi, C. Hu, ACS Appl. Mater. Interfaces 8 (2016) 736–744.
[97] J. Kim, H. Ryu, J.H. Lee, U. Khan, S.S. Kwak, H.J. Yoon, S.W. Kim, Adv. Energy Mater. 10 (2020) 1903524.
[98] H.L. Wang, Z.H. Guo, G. Zhu, X. Pu, Z.L. Wang, ACS Nano 15 (2021) 7513–7521.
[99] L.K. Anlin, K.V. Vijoy, K. Pradeesh, S. Thomas, H. John, K.J. Saji, Phys. B Condens. Matter 639 (2022), 413952.
[100] Z. Song, W. Li, H. Kong, Y. Bao, N. Wang, W. Wang, Y. Ma, Y. He, S. Gan, L. Niu, Nano Energy 92 (2022), 106759.
[101] J. Chun, J.W. Kim, W.-s Jung, C.-Y. Kang, S.-W. Kim, Z.L. Wang, J.M. Baik, Energy Environ. Sci. 8 (2015) 3006–3012.
[102] Y.-h Zhang, Y. Shao, C. Luo, H.-z Ma, H. Yu, X. Liu, B. Yin, J.-l Wu, M.-b Yang, J. Mater. Chem. C 11 (2023) 260–268.
[103] S. Pongampai, T. Charoonsuk, N. Pinpru, P. Pulphol, W. Vittayakorn, P. Pakawanit, N. Vittayakorn, Compos. Part B Eng. 208 (2021), 108602.
[104] Y. Zou, J. Xu, K. Chen, J. Chen, Adv. Mater. Technol. 6 (2021), 2000916.
[105] F.R. Fan, L. Lin, G. Zhu, W. Wu, R. Zhang, Z.L. Wang, Nano Lett. 12 (2012) 3109–3114.
[106] Y.K. Pang, X.H. Li, M.X. Chen, C.B. Han, C. Zhang, Z.L. Wang, ACS Appl. Mater. Interfaces 7 (2015) 19076–19082.
[107] J. Huang, X. Fu, G. Liu, S. Xu, X. Li, C. Zhang, L. Jiang, Nano Energy 62 (2019) 638–644.
[108] R. Wang, S. Gao, Z. Yang, Y. Li, W. Chen, B. Wu, W. Wu, Adv. Mater. 30 (2018), 1706267.
[109] Q. Zheng, L. Fang, H. Guo, K. Yang, Z. Cai, M.A.B. Meador, S. Gong, Adv. Funct. Mater. 28 (2018), 1706365.
[110] W. Li, Y. Pei, C. Zhang, A.G.P. Kottapalli, Nano Energy 84 (2021), 105865.
[111] M. Mayer, X. Xiao, J. Yin, G. Chen, J. Xu, J. Chen, Adv. Electron. Mater. 8 (2022), 2200782.

[112] X. Shi, Y. Wei, R. Yan, L. Hu, J. Zhi, B. Tang, Y. Li, Z. Yao, C. Shi, H.-D. Yu, W. Huang, Nano Energy 109 (2023), 108231.
[113] Q. Sun, L. Wang, X. Yue, L. Zhang, G. Ren, D. Li, H. Wang, Y. Han, L. Xiao, G. Lu, H.-D. Yu, W. Huang, Nano Energy 89 (2021), 106329.
[114] T. Charoonsuk, S. Supansomboon, P. Pakawanit, W. Vittayakorn, S. Pongampai, S. Woramongkolchai, N. Vittayakorn, Carbohydr. Polym. 297 (2022), 120070.
[115] M. Kang, M.S. Bin Mohammed Khusrin, Y.-J. Kim, B. Kim, B.J. Park, I. Hyun, I. M. Imani, B.-O. Choi, S.-W. Kim, Nano Energy 100 (2022), 107480.
[116] K. Xia, D. Wu, J. Fu, N.A. Hoque, Y. Ye, Z. Xu, Nano Energy 78 (2020), 105263.
[117] S. Roy, H.-U. Ko, P.K. Maji, L. Van Hai, J. Kim, Chem. Eng. J. 385 (2020), 123723.
[118] S. Chen, J. Jiang, F. Xu, S. Gong, Nano Energy 61 (2019) 69–77.
[119] S.H. Shin, Y.E. Bae, H.K. Moon, J. Kim, S.H. Choi, Y. Kim, H.J. Yoon, M.H. Lee, J. Nah, ACS Nano 11 (2017) 6131–6138.
[120] Y. Liu, Q. Fu, J. Mo, Y. Lu, C. Cai, B. Luo, S. Nie, Nano Energy 89 (2021), 106369.
[121] C. Ma, S. Gao, X. Gao, M. Wu, R. Wang, Y. Wang, Z. Tang, F. Fan, W. Wu, H. Wan, W. Wu, InfoMat 1 (2019) 116–125.
[122] S. Lee, B. Yeom, Y. Kim, J. Cho, Nano Energy 56 (2019) 1–15.
[123] H.G. Menge, N.D. Huynh, K. Choi, C. Cho, D. Choi, Y.T. Park, Adv. Funct. Mater. (2022) 2210571. DOI: 10.1002/adfm.202210571.
[124] Y. Han, Y. Han, X. Zhang, L. Li, C. Zhang, J. Liu, G. Lu, H.D. Yu, W. Huang, ACS Appl. Mater. Interfaces 12 (2020) 16442–16450.
[125] Q.M. Saqib, M.Y. Chougale, M.U. Khan, R.A. Shaukat, J. Kim, J. Bae, H.W. Lee, J.-I. Park, M.S. Kim, B.G. Lee, Nano Energy 89 (2021), 106458.
[126] H. Wang, L. Xu, Z. Wang, Nanoenergy Adv. 1 (2021) 32–57.
[127] Y. Pang, Y. Cao, M. Derakhshani, Y. Fang, Z.L. Wang, C. Cao, Matter 4 (2021) 116–143.
[128] C. Rodrigues, D. Nunes, D. Clemente, N. Mathias, J.M. Correia, P. Rosa-Santos, F. Taveira-Pinto, T. Morais, A. Pereira, J. Ventura, Energy Environ. Sci. 13 (2020) 2657–2683.
[129] Y. Pang, F. Xi, J. Luo, G. Liu, T. Guo, C. Zhang, RSC Adv. 8 (2018) 6719–6726.
[130] Y. Hu, Z. Zheng, Nano Energy 56 (2019) 16–24.
[131] J. Liu, L. Gu, N. Cui, Q. Xu, Y. Qin, R. Yang, Research 2019 (2019), 1091632.
[132] K. Dong, X. Peng, Z.L. Wang, Adv. Mater. 32 (2020), e1902549.
[133] Y. Yu, X.-X. Wang, G. Xie, J. Ma, T. Lv, K. Du, H. Hu, J. Zhang, Y. Li, Y.-Z. Long, K. Ruan, S. Ramakrishna, J. Mater. Chem. A 9 (2021) 24695–24703.
[134] H. He, J. Liu, Y. Wang, Y. Zhao, Y. Qin, Z. Zhu, Z. Yu, J. Wang, ACS Nano 16 (2022) 2953–2967.
[135] X. Tian, T. Hua, ACS Sustain. Chem. Eng. 9 (2021) 13356–13366.
[136] S. Wang, L. Lin, Z.L. Wang, Nano Energy 11 (2015) 436–462.
[137] J.-N. Kim, J. Lee, H. Lee, I.-K. Oh, Nano Energy 82 (2021), 105705.
[138] R. Guo, Y. Fang, Z. Wang, A. Libanori, X. Xiao, D. Wan, X. Cui, S. Sang, W. Zhang, H. Zhang, J. Chen, Adv. Funct. Mater. 32 (2022), 2204803.
[139] D. Lu, T. Liu, X. Meng, B. Luo, J. Yuan, Y. Liu, S. Zhang, C. Cai, C. Gao, J. Wang, S. Wang, S. Nie, Adv. Mater. 35 (2023), e2209117.
[140] D. Zhang, Y. Yang, Z. Xu, D. Wang, C. Du, J. Mater. Chem. A 10 (2022) 10935–10949.
[141] Y.-T. Jao, P.-K. Yang, C.-M. Chiu, Y.-J. Lin, S.-W. Chen, D. Choi, Z.-H. Lin, Nano Energy 50 (2018) 513–520.
[142] H. Zhang, D. Zhang, Z. Wang, G. Xi, R. Mao, Y. Ma, D. Wang, M. Tang, Z. Xu, H. Luan, ACS Appl. Mater. Interfaces 15 (2023) 5128–5138.
[143] Y. Li, S. Chen, H. Yan, H. Jiang, J. Luo, C. Zhang, Y. Pang, Y. Tan, Chem. Eng. J. 468 (2023), 143572.
[144] Y. Li, C. Wei, Y. Jiang, R. Cheng, Y. Zhang, C. Ning, K. Dong, Z.L. Wang, Adv. Fiber Mater. 4 (2022) 1584–1594.
[145] K.K. Fu, Z. Wang, J. Dai, M. Carter, L. Hu, Chem. Mater. 28 (2016) 3527–3539.
[146] S.W. Hwang, J.K. Song, X. Huang, H. Cheng, S.K. Kang, B.H. Kim, J.H. Kim, S. Yu, Y. Huang, J.A. Rogers, Adv. Mater. 26 (2014) 3905–3911.
[147] Q. Liang, Q. Zhang, X. Yan, X. Liao, L. Han, F. Yi, M. Ma, Y. Zhang, Adv. Mater. 29 (2017), 1604961.
[148] R. Pan, W. Xuan, J. Chen, S. Dong, H. Jin, X. Wang, H. Li, J. Luo, Nano Energy 45 (2018) 193–202.
[149] X. Peng, K. Dong, Y. Zhang, L. Wang, C. Wei, T. Lv, Z.L. Wang, Z. Wu, Adv. Funct. Mater. 32 (2022), 2112241.
[150] A. Yu, Y. Zhu, W. Wang, J. Zhai, Adv. Funct. Mater. 29 (2019), 1900098.
[151] L. Hu, P.L. Chee, S. Sugiarto, Y. Yu, C. Shi, R. Yan, Z. Yao, X. Shi, J. Zhi, D. Kai, H. D. Yu, W. Huang, Adv. Mater. (2023) 2205326.
[152] H. Dechiraju, M. Jia, L. Luo, M. Rolandi, Adv. Sustain. Syst. 6 (2021), 2100173.
[153] C. Zhou, T. Wu, X. Xie, G. Song, X. Ma, Q. Mu, Z. Huang, X. Liu, C. Sun, W. Xu, Eur. Polym. J. 177 (2022), 111454.
[154] F. Xi, Y. Pang, W. Li, T. Jiang, L. Zhang, T. Guo, G. Liu, C. Zhang, Z.L. Wang, Nano Energy 37 (2017) 168–176.
[155] W. Harmon, D. Bamgboje, H. Guo, T. Hu, Z.L. Wang, Nano Energy 71 (2020), 104642.
[156] C.M. Chiu, S.W. Chen, Y.P. Pao, M.Z. Huang, S.W. Chan, Z.H. Lin, Sci. Technol. Adv. Mater. 20 (2019) 964–971.
[157] K. Eom, Y.E. Shin, J.K. Kim, S.H. Joo, K. Kim, S.K. Kwak, H. Ko, J. Jin, S.J. Kang, Nano Lett. 20 (2020) 6651–6659.
[158] J. Sun, H. Choi, S. Cha, D. Ahn, M. Choi, S. Park, Y. Cho, J. Lee, T. e Park, J. J. Park, Adv. Funct. Mater. 32 (2021), 2109139.
[159] D. Lu, T. Liu, X. Meng, B. Luo, J. Yuan, Y. Liu, S. Zhang, C. Cai, C. Gao, J. Wang, S. Wang, S. Nie, Adv. Mater. 35 (2023), 2209117.
[160] T. Liu, M. Liu, S. Dou, J. Sun, Z. Cong, C. Jiang, C. Du, X. Pu, W. Hu, Z.L. Wang, ACS Nano 12 (2018) 2818–2826.
[161] K. Tao, Z. Chen, J. Yu, H. Zeng, J. Wu, Z. Wu, Q. Jia, P. Li, Y. Fu, H. Chang, W. Yuan, Adv. Sci. 9 (2022), e2104168.
[162] Y. Chen, C. Shi, J. Zhang, Y. Dai, Y. Su, B. Liao, M. Zhang, X. Tao, W. Zeng, Energy Technol. 10 (2022), 2200070.
[163] K. Hu, Z. Zhao, Y. Wang, L. Yu, K. Liu, H. Wu, L. Huang, L. Chen, Y. Ni, J. Mater. Chem. A 10 (2022) 12092–12103.
[164] T. Charoonsuk, S. Pongampai, P. Pakawanit, N. Vittayakorn, Nano Energy 89 (2021), 106430.
[165] R.K. Cheedarala, J.I. Song, Front. Nanotechnol. 3 (2021), 667453.
[166] J. Huang, Y. Hao, M. Zhao, H. Qiao, F. Huang, D. Li, Q. Wei, Compos. Part A Appl. Sci. Manuf. 146 (2021), 106412.
[167] W. Jiang, H. Li, Z. Liu, Z. Li, J. Tian, B. Shi, Y. Zou, H. Ouyang, C. Zhao, L. Zhao, R. Sun, H. Zheng, Y. Fan, Z.L. Wang, Z. Li, Adv. Mater. 30 (2018), e1801895.
[168] B. Liu, S. Wang, Z. Yuan, Z. Duan, Q. Zhao, Y. Zhang, Y. Su, Y. Jiang, G. Xie, H. Tai, Nano Energy 78 (2020), 105256.
[169] B.-H. Liu, G.-Z. Xie, C.-Z. Li, S. Wang, Z. Yuan, Z.-H. Duan, Y.-D. Jiang, H.-L. Tai, Rare Met. 40 (2021) 1995–2003.
[170] S. Shen, J. Yi, Z. Sun, Z. Guo, T. He, L. Ma, H. Li, J. Fu, C. Lee, Z.L. Wang, Nano-Micro Lett. 14 (2022), 225.
[171] O. Somseemee, P. Sae-Oui, C. Siriwong, Cellulose 29 (2022) 8675–8693.
[172] T.G. Weldemhret, D.-W. Lee, M.N. Prabhakar, Y.T. Park, J.I. Song, ACS Appl. Nano Mater. 5 (2022) 12464–12476.
[173] H. Xiang, J. Yang, X. Cao, N. Wang, Nano Energy 101 (2022), 107570.
[174] K. Yan, X. Li, X.-X. Wang, M. Yu, Z. Fan, S. Ramakrishna, H. Hu, Y.-Z. Long, J. Mater. Chem. A 8 (2020) 22745–22753.
[175] Z. Zheng, D. Yu, B. Wang, Y. Guo, Chem. Eng. J. 446 (2022), 137393.
[176] X. Han, D. Jiang, X. Qu, Y. Bai, Y. Cao, R. Luo, Z. Li, Materials 14 (2021) 1689.
[177] J. Ma, J. Zhu, P. Ma, Y. Jie, Z.L. Wang, X. Cao, ACS Energy Lett. 5 (2020) 3005–3011.